Seismic imaging of the eastern Algerian margin off Jijel: integrating wide-angle seismic modelling and multichannel seismic pre-stack depth migration

A. Mihoubi, P. Schnürle, Z. Benaïssa, M. Badsi, R. Bracene, H. Djelit, L. Geli, F. Sage, A. Agoudjil, F. Klingelhoefer

▶ **To cite this version:**

A. Mihoubi, P. Schnürle, Z. Benaïssa, M. Badsi, R. Bracene, et al.. Seismic imaging of the eastern Algerian margin off Jijel: integrating wide-angle seismic modelling and multichannel seismic pre-stack depth migration. Geophysical Journal International, 2014, 198 (3), pp.1486 - 1503. 10.1093/gji/ggu179 . hal-01859794

HAL Id: hal-01859794
https://hal.science/hal-01859794

Submitted on 19 Oct 2021

HAL is a multi-disciplinary open access archive for the deposit and dissemination of scientific research documents, whether they are published or not. The documents may come from teaching and research institutions in France or abroad, or from public or private research centers.

L'archive ouverte pluridisciplinaire **HAL**, est destinée au dépôt et à la diffusion de documents scientifiques de niveau recherche, publiés ou non, émanant des établissements d'enseignement et de recherche français ou étrangers, des laboratoires publics ou privés.

Distributed under a Creative Commons Attribution 4.0 International License

Geophysical Journal International

Geophys. J. Int. (2014) **198,** 1486–1503
GJI Geodynamics and tectonics

doi: 10.1093/gji/ggu179

Seismic imaging of the eastern Algerian margin off Jijel: integrating wide-angle seismic modelling and multichannel seismic pre-stack depth migration

A. Mihoubi,[1] P. Schnürle,[2] Z. Benaissa,[3] M. Badsi,[1] R. Bracene,[1] H. Djelit,[4] L. Geli,[2] F. Sage,[5] A. Agoudjil[1] and F. Klingelhoefer[2]

[1] *Algerian National Oil Company, Sonatrach/Exploration, Algeria. E-mail: abdelhafid.mihoubi@ep.sonatrach.dz*
[2] *Institut français de Recherche pour l'Exploitation de la Mer, France*
[3] *Université des Sciences et de la Technologie Houari Boumediene USTHB, Faculté des Sciences de la Terre, Algeria*
[4] *Centre de Recherche en Astronomie, Astrophysique et Géophysique CRAAG, Algeria*
[5] *Univ. Pierre et Marie Curie, Univ. Nice Sophia Antipolis, IRD, observatoire de la Côte d'Azur, CNRS, Géoazur, UMR F-7329, France*

Accepted 2014 May 13. Received 2014 May 8; in original form 2013 December 12

SUMMARY

This study presents the results of a deep seismic survey across the north Algerian margin, based on the combination of 2-D multichannel and wide-angle seismic data simultaneously recorded by 41 ocean bottom seismometers deployed along a north–south line extending 180 km off Jijel into the Algerian offshore basin, and 25 land stations deployed along a 100-km-long line, cutting through the Lesser Kabylia and the Tellian thrust-belt. The final model obtained using forward modelling of the wide-angle data and pre-stack depth migration of the seismic reflection data provides an unprecedented view of the sedimentary and crustal structure of the margin. The sedimentary layers in the Algerian basin are 3.75 km thick to the north and up to 4.5–5 km thick at the foot of the margin. They are characterized by seismic velocities from 1.9 to 3.8 km s^{-1}. Messinian salt formations are about 1 km thick in the study area, and are modelled and imaged using a velocity between 3.7 and 3.8 km s^{-1}. The crust in the deep sea basin is about 4.5 km thick and of oceanic origin, presenting two distinct layers with a high gradient upper crust (4.7–6.1 km s^{-1}) and a low gradient lower crust (6.2–7.1 km s^{-1}). The upper-mantle velocity is constrained to 7.9 km s^{-1}. The ocean–continent transition zone is very narrow between 15 and 20 km wide. The continental crust reaches 25 km thickness as imaged from the most landward station and thins to 5 km over a less than 70 km distance. The continental crust presents steep and asymmetric upper- and lower-crustal geometry, possibly due to either asymmetric rifting of the margin, an underplated body, or flow of lower crustal material towards the ocean basin. Present-time deformation, as imaged from three additional seismic profiles, is characterized by an interplay of gravity-driven mobile-salt creep and active thrusting at the foot of the tectonically inverted Algerian margin.

Key words: Tomography; Continental margins: divergent; Africa.

1 INTRODUCTION

This study presents a part of the SPIRAL project (Sismique Profonde et Investigations Régionales du Nord de l'Algérie). SPIRAL is an Algerian–French cooperation program between Sonatrach (Algerian national oil company), IFREMER (French Research Institute for Exploration of the Sea), UBO (University of Western Britanny, France), IUEM (European Institute for Marine Studies, France), CRAAG (Research Center on Astronomy, Astrophysics and Geophysics, Algeria), Géoazur (Sophia-Antipolis, France) and DGRSDT (General Direction of the Scientific Research and the Technological Development, Algeria). This project aims at studying the deep structure of the Algerian margin by a combined approach of multichannel seismic (MCS) and wide-angle techniques, in order to answer questions about the nature and architecture of the Algerian deep sea basin and continental margin. We present new knowledge concerning the nature and thickness of the crust and the continent–ocean transition zone off Jijel. Then the relation between superficial sedimentary formations and deep crustal structures will be examined. In particular, the presence of salt, its distribution and interplay with sedimentary processes and regional tectonics will be addressed. High resolution seismic data have been acquired along

© The Authors 2014. Published by Oxford University Press on behalf of The Royal Astronomical Society.

Downloaded from https://academic.oup.com/gji/article/198/3/1486/583506 by CNRS - ISTO user on 19 October 2021

Algerian margin during the Maradja 2003 (Domzig *et al.* 2006) and Maradja-Samra 2005 (Kherroubi *et al.* 2009) cruises. It was a high resolution acquisition but without a deep investigation (about 3–4 km). Deep structure in this area had not been studied with large-offset seismic data. During the SPIRAL Project, a total of five transects combining MCS and wide-angle seismic were acquired: to the west in the area of Mostaganem city (Badji *et al.* 2013), Tipaza (Leprêtre *et al.* 2013), Great Kabylia (Aidi *et al.* 2013) and to the east off Annaba city (Bouyahiaoui *et al.* 2013). Here, we present the specific results obtained along the 280-km-long, north–south, onshore-offshore profile that was acquired off Jijel city, in the area of the Lesser Kabylia.

2 GEOLOGICAL SETTING

The study area, eastern Algerian margin, includes onshore and offshore domains (Fig. 1). The onshore part is composed of several geological well-described series. These series are made of crystalline, sedimentary and magmatic formations. The crystalline units are a part of the AlKaPeCa blocks (for Alboran, Kabylies, Peloritan and Calabria; Bouillin 1986) and represent the internal zones in the study area (Bouillin & Raoult 1971; Bouillin 1977, 1986; Raoult 1975; Vila 1980; Djelit 1987; Mahdjoub 1990). These metamorphic units are made of khondalite and kinzigite gneisses at the lower part and phyllites at the upper units and are separated by a cataclastic unit (Djelit 1987). The Kabylian Oligo-Miocene (Aquitano-Burdigalian) unit rests unconformably on the crystalline basement and is composed of conglomerate, sandstone, marlstone, limestone and silexites (Raoult 1969; Bouillin 1977). In some regions it supports an olistostrum of Mauretanian, Massylien and Tellian or Numidian flyschs. The olistostrum includes tectono-sedimentary formations that consist of allogenes debris of highly variable size that have slided onto the bottom of the sea (Bouillin *et al.* 1977; Durand-Delga & Fontboté 1980; Vila 1980; Wildi 1983; Djelit 1987). All the formations described above in Lesser Kabylia are allochtonuous tectonics units with mainly southwards vergence. In the Jijel onshore area, the outcrops include also the Miocene (Burdigalian) and are made of marl and sandstone covered by the Pliocene (detritic bluish marl). In addition to metamorphic and sedimentary formations, the Lesser Kabylia is characterised by a series of serpentinized acidic, basic and ultrabasic igneous rocks (Benali 2007). External zones are represented in the study area by the Tellian nappes (Vila 1980). The offshore geological formations are deduced from seismic data and we distinguish from top to bottom:

(1) Thick Pliocene–Quaternary deposits at the foot of the margin to be thinning towards the north. DSDP site 371 (Deep Sea Drilling Project) borehole has been drilled in this area and proved a complete Pliocene–Quaternary sequence. The drill through 551 m of sediments in a water depth of 2792 m reached Messinian evaporites (Hsü *et al.* 1973; Mauffret *et al.* 2004).

(2) Messinian Upper Unit placed between the Messinian Mobile Unit and the Pliocene–Quaternary.

(3) Thick pre-Messinian sequences in the abyssal plain and its thick Miocene cover, supported by an undifferentiated basement, are dipping towards the south (Mauffret *et al.* 2007).

These sedimentary series are reduced or disappear to the south where the basement crops out.

This geological setting is directly related to the geodynamic evolution of western Mediterranean region. Extension in the western Mediterranean began 32–30 Ma and was mainly controlled by the subduction rollback and closure of Tethys Ocean under the European Plate (Frizon de Lamotte *et al.* 2000). In the subduction backarc, the Algerian offshore basins were progressively formed from north to south (Rosenbaum *et al.* 2002), with stretching starting possibly in late Oligocene–early Miocene times (Rosenbaum & Lister 2004). The opening of these basins induced the detachment of a part of the south-European margin which was transported towards the south and accreted to the African Plate. These terranes are called AlKaPeCa domain and constitute the internal zones of the Algerian margin. Spreading of the Algerian basin ceased during the Burdigalian–Langhian time (15 Ma), as indicated by the chemical change in volcanism along the Algerian margin (Maury *et al.* 2000). The Algerian basin is often presented as an extension of the Provencal basin that has undergone a similar history together with a drift of the internal domain of Maghrebian system (Kabylides) towards the southeast (Mauffret *et al.* 2004). The Provençal basin opened as a back-arc basin behind the Corsica–Sardinian block between 19 and 16 Ma (e.g. Speranza *et al.* 2002). Less than 6 Ma the Mediterranean has undergone rapid and dramatic palaeo-environmental changes known as the Messinian salinity crisis (Hsü *et al.* 1973). This event (∼5.96–5.32 Ma, e.g. Gautier *et al.* 1994; Krijgsman *et al.* 1999) resulted from the progressive closure of the two-way connection between the Atlantic Ocean and Mediterranean sea (Benson *et al.* 1991; Krijgsman *et al.* 1999; Govers 2009). Among the most important characteristics of this event, reducing the supply of water from the Atlantic Ocean resulted in increased salinity and the deposition of thick evaporitic sequences (e.g. Lofi *et al.* 2011). These Messinian sequences were imaged using high resolution, low penetration (<3 km) seismic profiling acquired along the whole Algerian margin during the Maradja 1 and Maradja 2 surveys (Domzig *et al.* 2006; Kherroubi *et al.* 2009). The Algerian margin is an active plate boundary and is related to the convergence between Africa and Europe. The convergence rate is estimated to be around 2–3 mm yr^{-1} (Calais *et al.* 2003). In Northern Algeria (onshore and offshore), seismicity is active with moderate to low magnitude earthquakes (Harbi *et al.* 1999), mostly focused along the southern suture between the internal and external domains (Yelles *et al.* 2009). The largest recorded seismic event in this this region was the Djidjelli earthquake of 1856 August 22. This represents the strongest felt and recorded seismic event in the coastal zone of the eastern part of Algeria. It was preceded by a large foreshock which occurred on 1856 August 21 and it was felt as far as Alger, Sétif, Batna and la Calle, Baléares isles (Spain) and Genoa (Italy) (Harbi *et al.* 1999 and 2003). In order to explore the surrounding area of this earthquake, Yelles *et al.* (2009) have identified three overlapping thrust-fault segments, oriented NE–SW to E–W in the lower slope and near the foot of the slope, from the high bathymetric and resolution seismic Maradja2 survey and from one industry seismic profile. Using the rupture zones of the identified segments, modelling of the tsunami of 1856 August 21–22 was performed. Evidence of reverse faulting is mainly related to basement topography as well as an asymmetrical fold which produces the growth of a basin on its backlimb that is tilted towards the continent (Yelles *et al.* 2009). The four seismic profiles analysed in this study offer the opportunity to re-examine the complex interplay between compressional and salt tectonics and to verify the present-time inversion of the Algerian margin.

3 DATA ACQUISITION

The deep seismic data used in this study were acquired during the SPIRAL cruise conducted on board R/V L'Atalante (IFREMER) in

Downloaded from https://academic.oup.com/gji/article/198/3/1486/583506 by CNRS - ISTO user on 19 October 2021

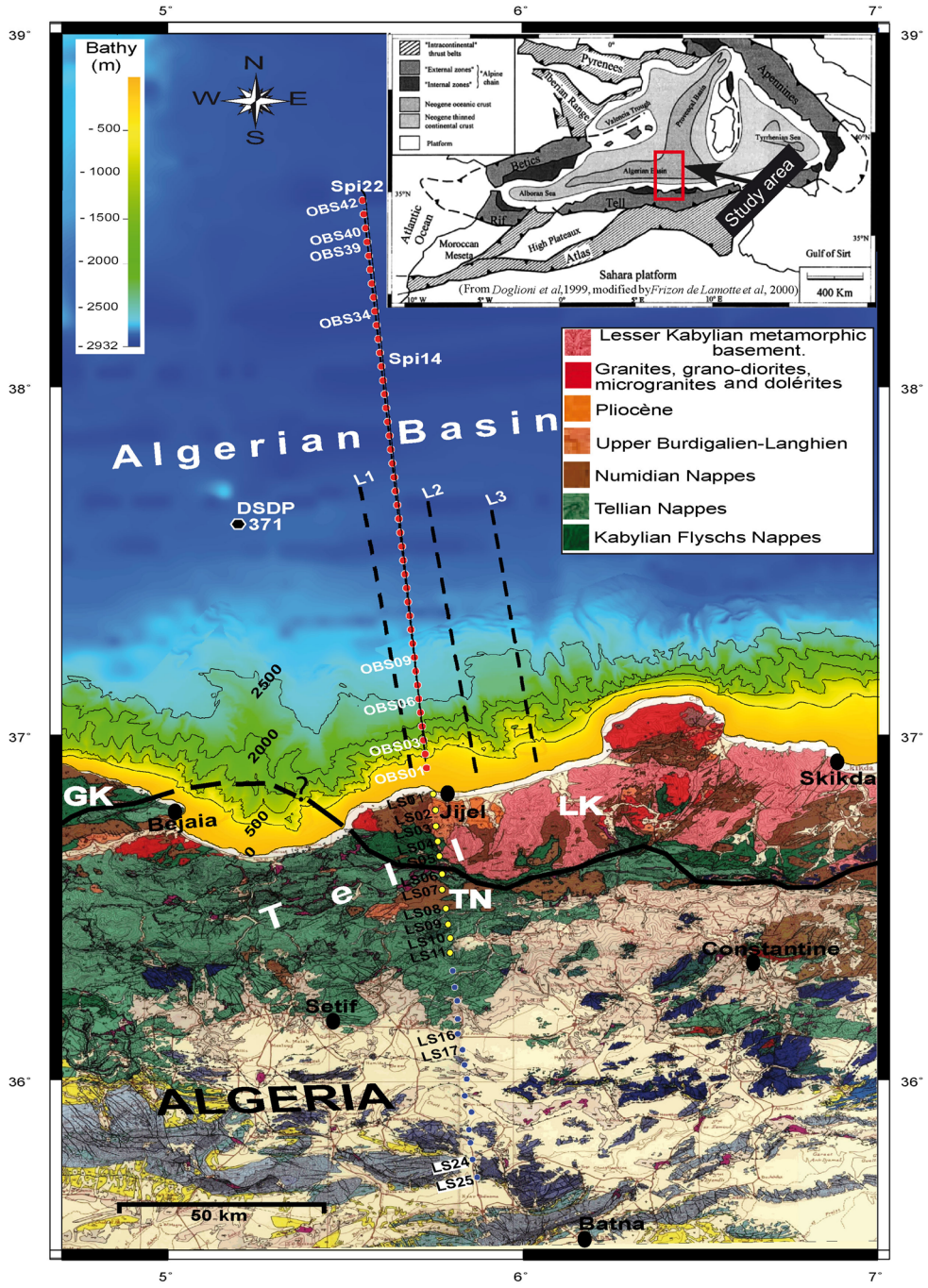

Figure 1. Eastern Algeria geological map showing the different structural units of the onshore part of the study area (after Vila 1980). The main structural domains (Bouillin 1977; Vila 1980; Wildi 1983): Lesser and Great Kabylia, LK and GK, (internal zones) and Tellian nappes, TN, (external zones). The limit between the internal and the external zones is marked by a black line. For the offshore part, the bathymetry is extracted from the Maradja surveys and ETOPO1 1-minute global relief (www.ngdc.noaa.gov). The multichannel seismic profiles Spi14 and Spi22 of this wide-angle survey are marked by black lines. Locations of ocean bottom seismometers (OBS) are indicated by red circles, and land stations by yellow circles (good signal-to-noise ratio) and blue circles (noisy data). The multichannel seismic profiles L1, L2 and L3 from Algeria offshore 2-D seismic survey are localized with black dashed lines.

2009 October–November. It consists of a sea-land wide-angle experiment, using 42 ocean bottom seismometer (OBS) and 25 broad-band land stations (LS) deployed along a north–south trending line (Fig. 1). For the onshore side, 25 three-components broad-band stations (from CRAAG) were deployed along 100 km from the Jijilian coast across Lesser Kabylia (Jijel and Mila) to the Tellian thrustbelt (Setif and Batna). On the offshore side it extends 180 km northwards of Jijel, in the Algerian basin. The average OBS and land-station spacings were 4.4 and 5 km, respectively. The seismic source was specifically designed to image the deepest crustal structures. It consisted in an air-gun array, with a total volume of 8909 cubic inches, towed at an average 29 m depth. The shot spacing was 60 s (resulting in an average distance of ∼150 m between shots), and 1205 shots were fired. Simultaneously, the shots were recorded on a 4.5-km-long streamer, composed of 360 channels, spaced at 12.5 m interval, enabling the acquisition of a low-resolution 2-D

Downloaded from https://academic.oup.com/gji/article/198/3/1486/583506 by CNRS - ISTO user on 19 October 2021

multichannel seismic profile, Spi22. In order to improve the MCS imaging, a coincident 2-D multichannel seismic line, Spi14, was also acquired using the same streamer but a different source array. In order to improve the seismic fold, the shot spacing was reduced to 50 m and 3520 shots were fired. The air-gun array was synchronized on the first bubble to enhance deep frequencies (single bubble array; Avedik *et al.* 1993) using a total volume of 3040 cubic inches. In order to improve the seismic imaging of our study area and to constrain lateral variations, three additional 2-D multichannel seismic lines, sub-parallel to the wide-angle profile and at a distance of about 15 km on either side, have been provided by the Sonatrach exploration division. These MCS profiles were acquired using a 3000 cubic inch air-gun array at 1950 psi pressure, towed at 6 m depth with a 25 m shot-point interval, and 6000 km long streamer of 480 channels towed at 8 m depth. Simultaneously, during the SPIRAL cruise, additional data were acquired along all MCS profiles, including: magnetic, gravity and bathymetry data. Gravity data was acquired by a LOCKHEED MARTIN BGM-5 IFREMER. Measurements are provided every 10 s with an accuracy of 1mGal (10^{-5} m s^{-2}). Using a SeaSPY magnetometer, magnetic data were recorded. The measurement accuracy is about 0.2 nT. Also further gravimetric data from Sonatrach have been used in this study.

4 DATA PROCESSING

4.1 MCS data

The main goal of the data processing workflow was to prepare pre-stack depth migrated (PSDM) gathers suitable for velocity refinement and horizon adjustment in depth. First, conventional processing in the time domain was performed using the Geocluster (CGG) processing software at 4 ms time sampling interval for 6.25 m Common Depth-Point (CDP) spacing. An accurate time and space inverse Q filtering was applied in the pre-stack domain. Because of the single bubble source, the signature was converted to minimum phase prior to deconvolution. Then a pre-stack surface-consistent deconvolution was applied to improve the temporal resolution followed by a zero phase conversion. Conventional normal moveout (NMO) velocity analysis was then performed on every 500th CDP gather. For each velocity location, multivelocity function stack, semblances and gathers were displayed interactively, allowing stack velocities to be determined. Percentage stacks and NMO corrected gathers were then produced to check the validity of the picks. This procedure was applied several times in separate phases during the processing. The data contained significant amounts of unwanted coherent and random noise. These noise events were both analysed and attenuated in the offset domain. Finally, bandpass frequency filtering and Kirchhoff post-stack time migration were applied.

4.2 OBS and land-station data

The processing sequence of the wide-angle data once downloaded from the instruments included: OBS's internal clock-drift correction; OBS's relocation on the seafloor from traveltime picks of water-wave direct arrivals; instrument positioning on a great-circle arc and definition of 2-D geometry; filtering to attenuate low-frequency noise; signal deconvolution, to sharpen the wavelet and enhance the frequency content. In order to preserve the gain contrast between the first and secondary arrivals, no automatic gain control (AGC) was applied, but a scale proportional to offset was used. In addition, an FX deconvolution (in a moving 1.9 s $\times$ 21 traces window) was applied to the onshore station data in order to attenuate the higher noise levels when compared to OBS. The land stations can be divided into two groups concerning the data quality: the first eleven stations from the coast to approximately 50–60 km southward (Fig. 1) present good signal to noise ratio, while stations 12–25 recorded only noise. The absence of signal may be related to a near-surface site effect or a more distant structural obstacle to seismic wave propagation, however it is not related to instruments malfunctioning.

4.3 Magnetic and gravity

The magnetic and gravity measurements were processed with the Caraïbes software (IFREMER). The magnetic anomaly was computed against the IGRF 2005 model. The processing sequence applied for gravity data contain: Unit conversion, data merge with navigation, offset correction, Eötvös correction, instrument lag correction, latitude correction and base tie calculation, Bouguer correction, Bouguer gravity, data quality assessment and along-line gravity filtering and final editing.

5 METHODOLOGY

In this study, our approach is a joint inversion of wide-angle records and multichannel seismic data. The 2-D model (with x = horizontal distance along profile and z = depth) is parametrized with interfaces (seismic horizons) that are representative for geological units, and interval velocity nodes at the top and the bottom of each layer. The interface depth and the velocities are inverted iteratively from top to bottom until: (i) a satisfactory fit between calculated and observed traveltimes on OBS and land stations is obtained and (ii) common-offset classes reach flattening after pre-stack depth migration. The iterative sequence is not an automatic process: instead, at each iteration, we manually refine both interface-depth and velocities in order to achieve a model that includes all geological knowledge. A minimum structure approach has been used during modelling of the crustal and upper mantle, where only depth and velocity nodes necessary to fit the data in the limits of the picking order. In the sedimentary layers the structures from reflection seismic modelling were included; however care was taken to not unnecessarily introduce lateral velocity gradients. Forward modelling of wide-angle traveltimes was performed using the RAYINVR software (Zelt & Smith 1992), for 2-D ray tracing and traveltime inversion. The PSDM processing was undertaken using the Seismic Unix geophysical package (SU; Stockwell 1999a,b). The process is used to compute traveltime tables regularly spaced at 200 m along the profile by paraxial ray tracing on a 50 $\times$ 24 m spaced coarse grid, then traveltimes in shadow zones are compensated by solving the eikonal equation. Migrated traces are output as CDP gathers binned at 25 m with 45 offset-classes between 227 and 4627 m at 100 m spacing. Residual moveout (RMO) of migrated gathers is converted to interval velocity updates (Liu & Bleistein 1995). The residual moveout behaviour together with the seismic character from PSDM images are a key to locate accurately major geological contacts, moreover with higher horizontal resolution when compared to OBS records. The workflow of our velocity refinement approach is summarised in Fig. 2. In a similar way, OBS records of the upward travelling primary waves reflected from the subsurface are migrated using an additional traveltime table computed at the OBS sea-bottom location. Furthermore, mirror imaging (e.g. Dash *et al.* 2009) is performed by migrating first (receiver-side) sea-surface

Downloaded from https://academic.oup.com/gji/article/198/3/1486/583506 by CNRS - ISTO user on 19 October 2021

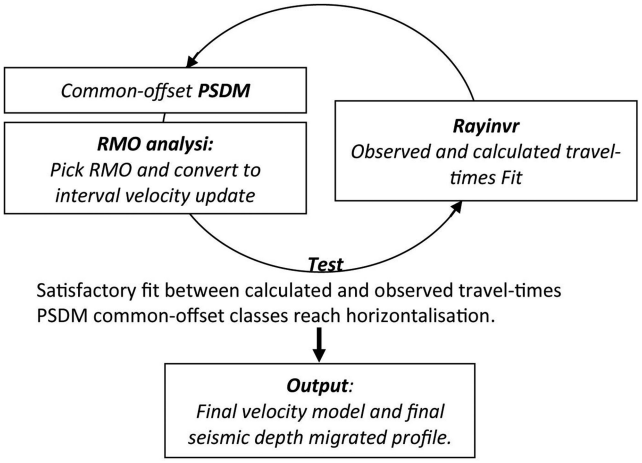

Figure 2. Velocity refinement workflow based on pre-stack depth migration using the seismic Unix geophysical package (SU) and forward modelling of wide-angle traveltime of the RAYINVR program (Zelt & Smith 1992).

related multiple on OBS records (downward travelling waves) using a traveltime table computed at OBS mirror location (the sea-bottom depth above sea-level). Finally, the 2 migrated OBS profiles of up and downward travelling waves are stacked to produce the final section. An initial up-downward travelling wave separation (e.g. Schneider & Backus 1964) performed by combining hydrophone and vertical OBS components is not presented herein as it did not improve significantly the seismic image.

On the three additional MCS profiles, the same key interfaces have been digitized and an estimate of each concurrent velocity model was built from our wide-angle model by copying its velocity nodes onto the new interfaces. This model was then used to transform the processed sections from time to depth.

In order to verify the consistency of the velocity model with gravity data, the free-air anomaly was modelled using the GRAVMOD software (Zelt & Smith 1992). The densities used for the gravity modelling are based on the empirical relationship between seismic velocity and density by Ludwig *et al.* (1970), except for the continental part where Christensen & Mooney (1995) relationship between velocity and density was used. In order to avoid edge effects, the model was extended 100 km at both ends and to a depth of 90 km. The mantle density was set to a constant 3300 kg m^{-3} (Fowler 1990).

6 DATA ANALYSIS

Representative data records are displayed in Fig. 3, for OBS3, OBS13 and OBS34 and for land station LS05. Right below OBS34 and OBS13 (Figs 3a and b), the uppermost sedimentary sequence is nearly transparent, and dominated by the water-wave source oscillations. At the base of this sequence, high amplitude reflections (PsP1) and a sharp refracted event (Ps1, with an apparent velocity above 3 km s^{-1}) are observed. Ps1 does generally not extend beyond 10 km offset. The base of this high amplitude sequence is marked by a sharp reflection, named PsP2.

On both sides of OBS34, a gap characterised by the absence of refracted arrivals is observed between the Ps1 and Pg1 branches (Fig. 3a). This gap is also present on all data records, from OBS42 to OBS14, indicating a velocity inversion in the underlying layers. In contrast, on OBS13 (Fig. 3b) the absence of refracted arrival is observed only on the northern side (negative offset), while on the southern side (positive offset) Ps1 is followed by refractions

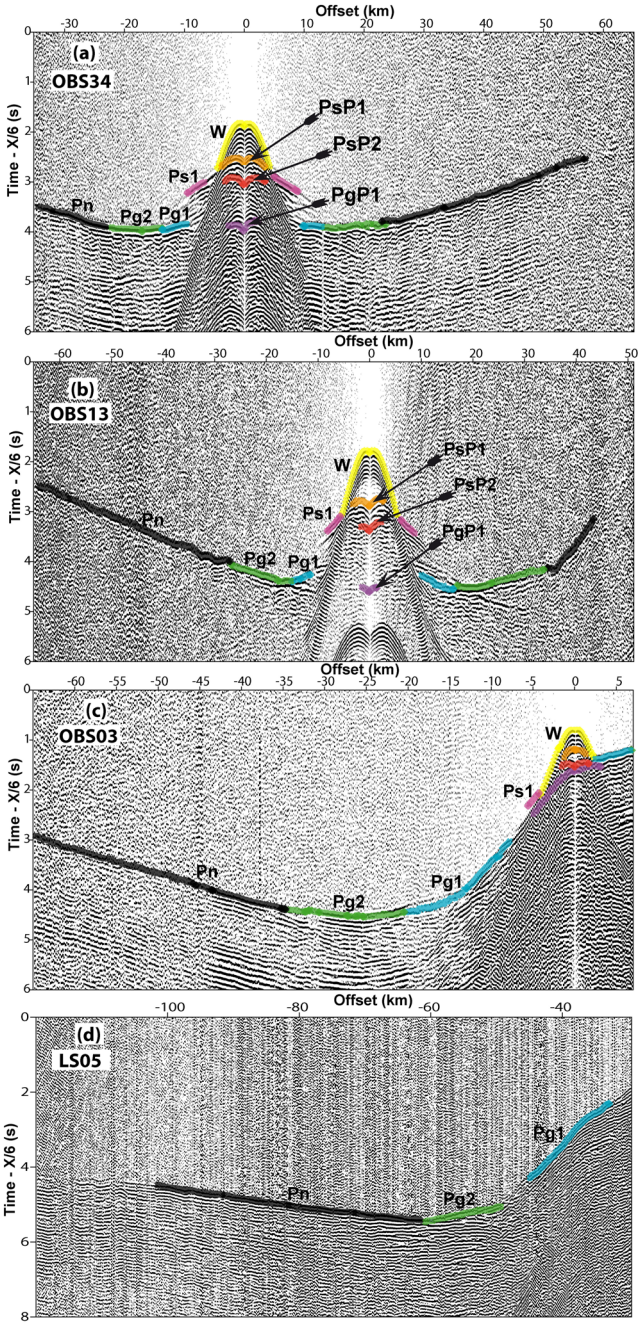

Figure 3. Examples of representative OBS and land station data records along the Jijel wide-angle profile: (a) OBS34, (b) OBS13, (c) OBS03 and (d) LS05. Bandpass filter (4–18 Hz), deconvolution, offset gain recovery, mute and 6 km s^{-1} velocity reduction have been applied. The identified phases are: water (W); refraction in the Messinian unit (Ps1); reflection at the top of the Messinian mobile unit (PsP1); reflection at the base of the Messinian mobile unit (PsP2); refraction in the upper crust (Pg1); refraction in the lower crust (Pg2); reflection at the top of the basement (PgP1) and refraction in the upper mantle (Pn).

with decreasing apparent velocities above a compact sequence of refracted events (Pg1) on top of a layer characterised by a high apparent velocity. This compact sequence is present and thickens from OBS13 to OBS4 at the continental rise near the foot of the Lesser Kabylia slope. On the slope, from OBS3 to OBS01, an almost continuous train of refracted events connects Ps1 to Pg1 (Fig. 3c). Two crustal refracted arrivals follow, Pg1 and Pg2, from the top of layers

Downloaded from https://academic.oup.com/gji/article/198/3/1486/583506 by CNRS - ISTO user on 19 October 2021

characterised by distinct apparent velocities, ranging from 4.5 to 5 km s^{-1} and from 5.5 to 6.5 km s^{-1}, respectively (Fig. 3). These arrivals are of high amplitude and clearly visible on all 42 OBS sections. Often, a reflection PgP1 associated to the Pg1 refraction can be identified. Only few PmP reflected waves from the Moho could be identified, for instance on OBS3 or LS05 (Fig. 3d). Sedimentary reflected arrivals are better observed on the hydrophone channel while refracted waves are more distinct on the vertical component. The refracted wave Pn from the mantle is observed with high confidence, at offsets of up to 80 km on OBSs and larger than 100 km on land station data records.

7 RESULTS

7.1 Velocity refinement by multichannel seismic pre-stack depth migration

Along the entire Algerian margin, the Messinian units represent key markers that help identify and delimit the major geological sequences. On top of the Messinian units, the Plio-Quaternary sequence appears as weakly deformed compact sequence with relatively weak seismic impedance (almost transparent at times), easily identifiable on the MCS (Figs 4a and b) and OBS (Fig. 4d) data. The Messinian sequence is composed of the Upper Unit (UU) and the Mobile Unit (MU). The seismic character of the UU is known to consist in high amplitude coherent reflections on the MCS data, while the MU appears as more heterogeneous and is associated to chaotic and discontinuous seismic events: on the OBS data, the high amplitude reflection PsP1 corresponds to the top of the MU, rather than the top of the UU. Hence, the pre-stack depth migration OBS gathers allows to better identify the MU (Fig. 4d). Moreover, pre-stack depth migrated CDP gathers show, that the MU are characterised by high seismic velocities of 3.7–3.8 km s^{-1}, a proof for high content of massive salt. The UU present much lower velocities from 2.3 to 2.9 km s^{-1}, with a vertical velocity gradient comparable to that of the Plio-Quaternary deposited on top. Therefore in our model, the first layer incorporates both the Plio-Quaternary and UU, and we achieve flat RMO gathers with 1.9 and 2.9 km s^{-1} at layer top and base, respectively (Fig. 4c).

The pre-Messinian formations are poorly imaged along most of the profile, presenting week acoustic reflections: the top of the acoustic basement (the crust in the Algerian basin) is difficult to identify unequivocally on both, MCS and OBS data. Furthermore, the gap in refracted arrivals from the pre-Messinian units in the OBS data records does not allow to quantify the depth and the velocity of this layer. The RMO gathers are a key to define the pre-Messinian velocities and the depth of the top of the basement: we define the bottom of the pre-Messinian unit as the zone where flattened reflected events disappear (Fig. 4c). RMO gathers are flattened with velocities ranging from 2.95 to 3.05 km s^{-1} at the top and 3.5–3.65 km s^{-1} at the base of the pre-Messinian unit. The deep part of the model (crust and mantle) is solely constrained by the analysis of OBS records, as the MCS data does not exhibit many coherent seismic reflections from the crust and from the Moho.

7.2 *P*-wave velocity: Modelling of the wide-angle data

The final *P*-wave velocity model is 28 km deep and 240 km long, including 186 km offshore and 54 km onshore (Fig. 6). The model comprises seven layers: water, the Plio-Quaternary and upper unit of Messinian evaporates (UU), the Mobile unit of the Messinian sequence (MU), the upper crust, the lower crust, and the mantle. The salt layer is constrained by two reflection arrivals (PsP1 and PsP2) and one refraction (Ps1). The crustal layers and the Moho are constrained by refractions Pg1 and Pg2, and by reflections PgP1 (Fig. 3). The contact between the Kabylian basement and the sedimentary basin at the foot of the margin is constrained by OBS03–OBS08: rays that are able to turn in the sedimentary basin on OBS07 and OBS08 are guided by the fast basement before turning in the basin towards OBS03–OBS06 (Figs 3 and 5). Furthermore, an approximately 1 km thick basin has developed on the continental shelf during Plio-Quaternary, as imaged on the MCS profiles and by the first four OBSs (OBS01–OBS04). Shots from the coastal region reaching land stations LS01 to LS05 constrain the same zone using reversed ray paths. The large offset arrivals from land stations contributed as a principal constraint in the modelling of the continental crustal velocity structure and the Moho depth. Delays in arrivals at LS05 to LS11 are accounted for by introducing a low velocity layer from LS05, where the Kabylian basement is known to crop out, to the southern end of the profile where its thickness approaches 2.5 km. In the absence of reverse shots during this experiment or other seismic surveys acquired over this unit, its precise geometry and velocity structure remains undefined and this basin can be regarded as a weathering layer. Finally, the deepest Pn refractions recorded at LS07–LS11 constrain the Moho depth to 24 km depth near 190 km distance along the profile. The fit between the picked and the predicted traveltimes is good throughout the complete model. The portion of the model in which it was most difficult to obtain a good fit corresponds to the foot of the margin, between OBS01 and OBS09. However, Fig. 5(b) shows the quality of the fit at OBS06 as example of this zone. The sedimentary layers in the basin are characterised by seismic velocities from 1.9 to 3.8 km s^{-1}. Messinian formations were modelled and imaged using a velocity between 3.7 and 3.8 km s^{-1}. The velocity of the oceanic crust in this region presents two distinct layers characterized by two velocity gradients from 4.7 to 6.1 km s^{-1} and 6.2 to 7.1 km s^{-1}. The upper-mantle velocity is about 7.9 km s^{-1} (Fig. 6). The continental crust is characterized by relatively a low crustal velocity gradient (5.8–6.8 km s^{-1}). The thickness of the thinned continental crust increases to 23 km and reaches 25 km depth towards southern-most illuminated part of the model (by Pn arrivals at LS10 and LS11).

7.3 Velocity uncertainty and resolution

The quality of the fit between predicted and observed traveltimes was evaluated by calculating the rms error and the χ^2 parameter. The χ^2 is defined as the rms traveltime misfit between the calculated and observed arrivals normalised to the picking error. The rms traveltime misfit obtained is 0.071 s with a χ^2 of 0.460 for a total of 24 122 picks. The number of picks used is around 90 per cent of the total: The number of picks of all sedimentary phases is 4129 (17 per cent) of the total, while 9162 picks (38 per cent) are used for crustal phases and 8085 picks (33.5 per cent) for the mantle. Thus, the deeper structures (crust and Moho) are constrained with confidence from reflected and refracted phases. The sedimentary portion of the model is constrained by depth migration RMO of the MCS data. The number of picked traveltime data points, the rms error between calculated and observed times and the χ^2 parameter for each layer are listed in Table 1.

The resolution of the final velocity model is a measure of the number of rays passing through a region of the model constrained by one particular velocity node and is therefore dependent on the

Downloaded from https://academic.oup.com/gji/article/198/3/1486/583506 by CNRS - ISTO user on 19 October 2021

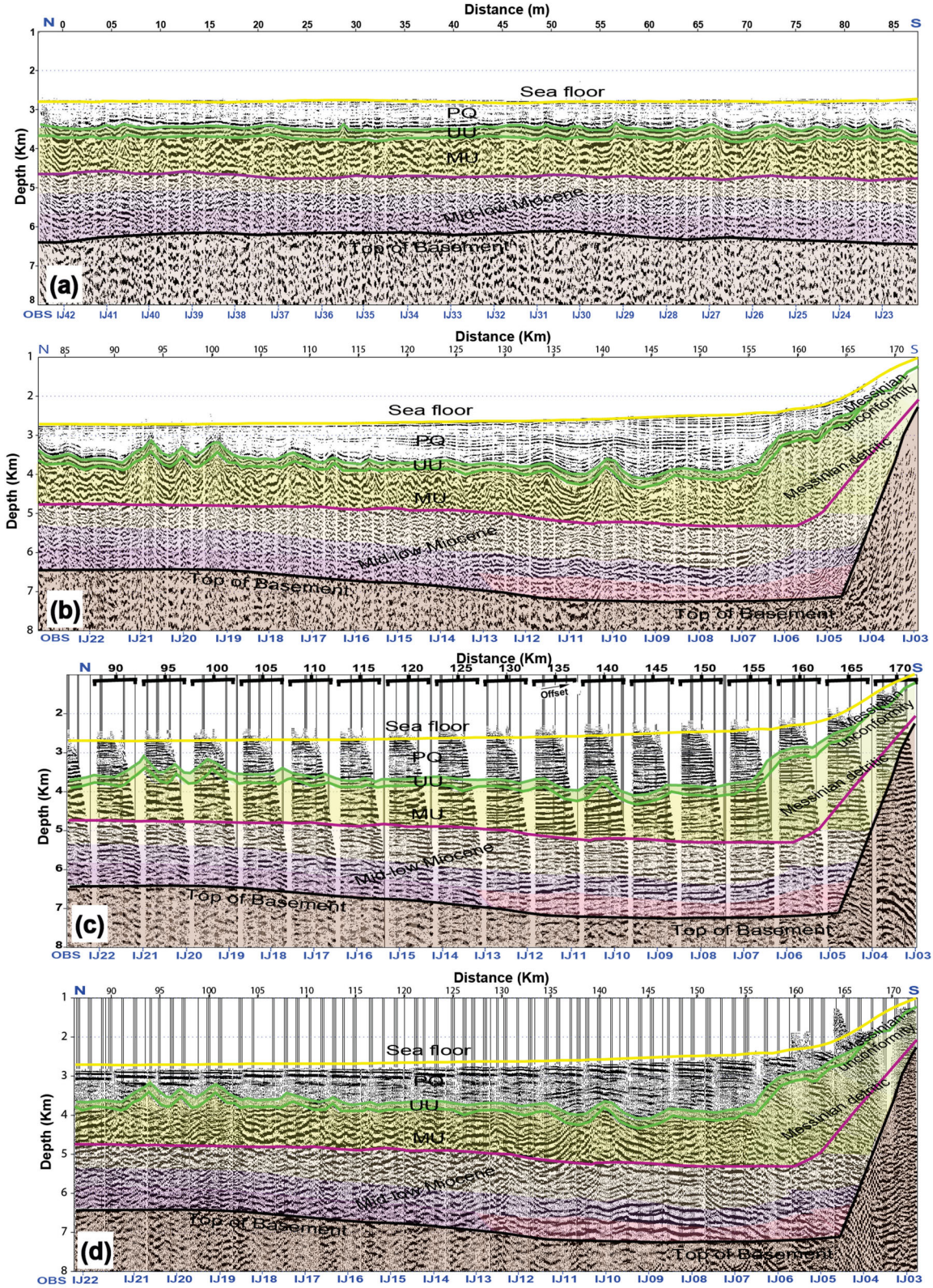

Figure 4. Pre-stack depth migration results: interfaces-velocity refinement and structural interpretation. Vertical exaggeration is 4. (a) Northern half of the pre-stack depth migrated Spi14, multichannel 2-D seismic (MCS) profile (see Fig. 1 for localization). PQ, Plio-quaternary; UU, upper unit of Messinian evaporates; MU, mobile unite of Messinian evaporites. Sea floor is indicated by yellow line and OBS locations are annotated at the bottom. (b) Southern half of the pre-stack depth migrated Spi14 MCS profile. (c) Depth migrated common depth point (CDP) gathers from the southern half of the Spi14 MCS profile. Overlay plot of 18 depth migrated CDP, spaced every 5 km. The horizontal CDP position along profile is at the center of each gather. Every trace in each gather corresponds to a migrated offset class; Offset within a gather increase from left to right. (d) Pre-stack depth migrated OBS hydrophone profile from the southern half (OBS03–OBS22) of the wide angle profile.

Downloaded from https://academic.oup.com/gji/article/198/3/1486/583506 by CNRS - ISTO user on 19 October 2021

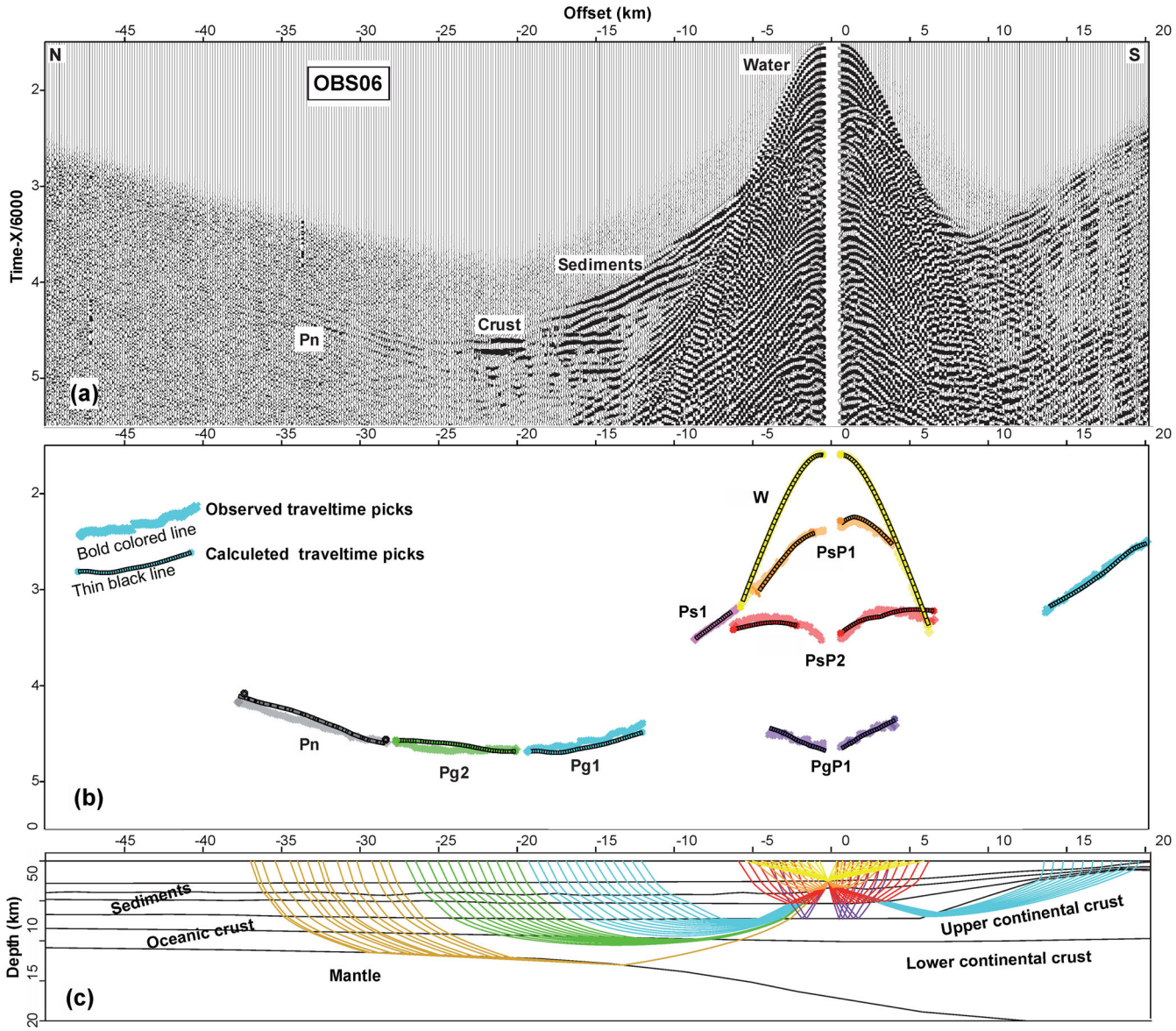

Figure 5. *P*-wave velocity modelling from wide-angle data. (a) Vertical component of selected record section (OBS06). The main observed arrivals are: water, sediment, crust refraction and mantle refraction Pn. A reduction velocity of 6 km s^{-1} was applied. (b) Superimposed of the observed and predicted traveltimes: Thin black line shows calculated traveltimes and bold coloured line shows the observed traveltimes picks. (c) Ray paths in the forward model.

node spacing (Zelt 1999; Fig. 7). Ideally, the diagonal terms of the resolution matrix are equal to one, but values of less than one indicate a spatial averaging of the true earth structure by a linear combination of model parameters (Zelt 1999). Typically, resolution matrix diagonals greater than 0.5–0.7 are said to indicate reasonably well-resolved model parameters (e.g. Lutter & Nowack 1990). The major part of the model has good resolution (>0.7) indicating that each velocity node is well-constrained. The gap in the OBS refracted phases from sediments below the salt layer explains the resolution decrease to a range of 0.5–0.7. The onshore sedimentary layers show resolution of less than 0.5 mainly because only Pg and Pn are observed in this area (Fig. 7) and sedimentary arrivals are missing due the large distance between the stations and the closest shot.

In order to estimate the velocity and depth uncertainty of the lower crustal structure and Moho geometry, a perturbation analysis was performed. Depth of the Moho and *P*-velocities at the base of the lower crustal layer were changed systematically. Then, the statistical *F*-test was applied in order to determine if the change between models is significant. Two zones were selected along the model: zone 1 extends between 60 and 100 km, where the model has a tabular geometry and the crust presents an oceanic velocity profile, while zone2 which extends from 115 to 155 km, where the Moho plunges under the Kabylian basement. Furthermore, zone 2 on the southern side is constrained by land stations and fewer OBSs than zone 1 (Fig. 7). At the boundaries of the perturbated zone, velocities where kept at the model's original value by an additionally inserted node, 5 km from the boundary. The 95 per cent confidence limit gives an estimation of the interval, where the perturbed model is significantly different from the original model. Results from this analysis show on one hand that an increase in the Moho depth together with a proportional increase of lower-crustal velocity (i.e. decreasing the velocity contrast at the Moho)

Downloaded from https://academic.oup.com/gji/article/198/3/1486/583506 by CNRS - ISTO user on 19 October 2021

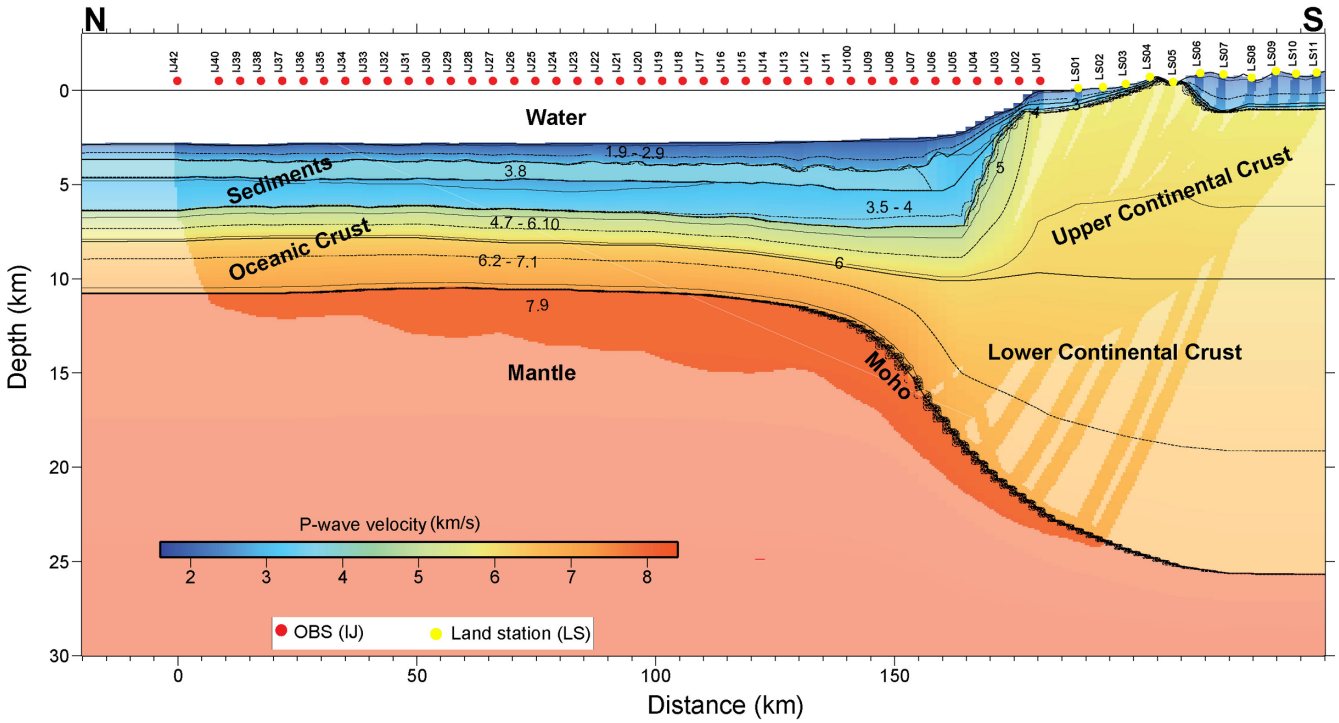

Figure 6. Final *P*-wave velocity model from forward modelling, using 41 OBS and 11 land stations. Vertical exaggeration is 4. Red circle indicates locations of the OBS and yellow circles indicate locations of the land stations. Isovelocity contours are represented every 0.5 km s^{-1}. Darker shaded areas show ray paths from the modelling and hence regions of the model that are constrained.

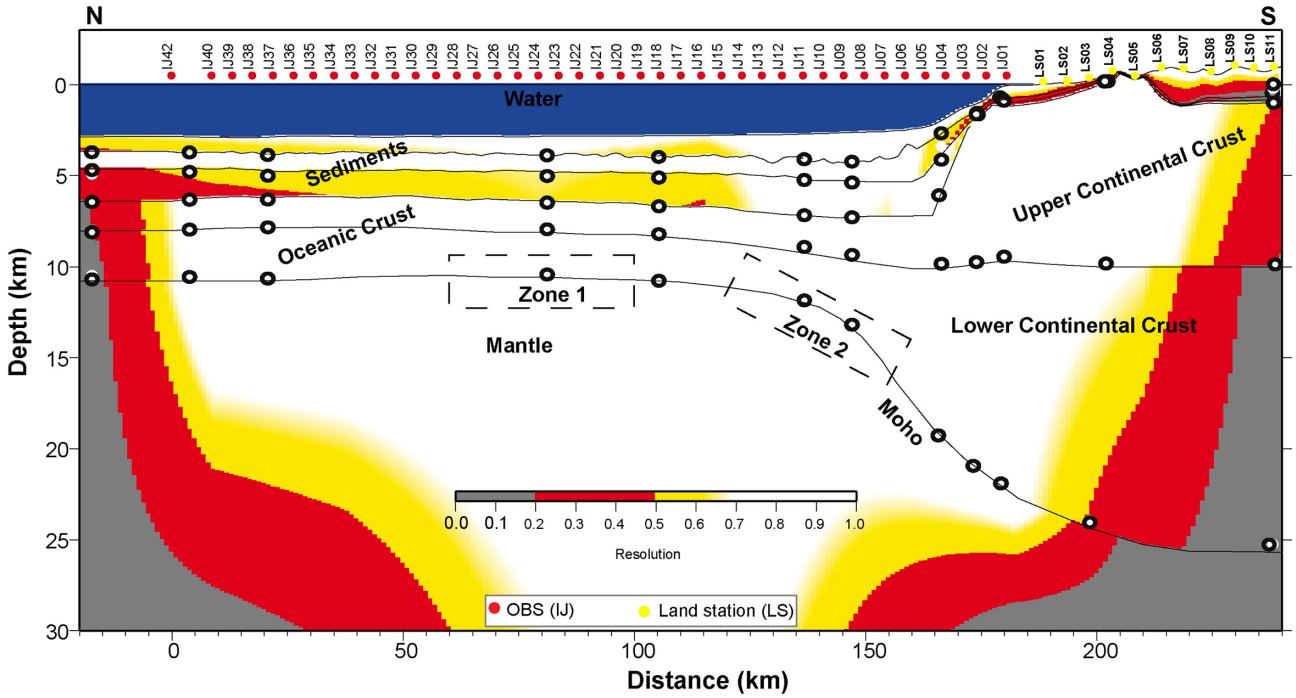

Figure 7. Resolution parameter for all velocity nodes. The areas coloured in white and yellow can be considered well resolved. A value above 0.5 is considered acceptable (Zelt 1999). Blue indicates the sea water layer. Velocity nodes are marked by circles. Vertical exaggeration is 4.

Downloaded from https://academic.oup.com/gji/article/198/3/1486/583506 by CNRS - ISTO user on 19 October 2021

Table 1. Traveltime residuals and χ^2 error for all phases and the complete model: Phases used in the modelling (see Fig. 3 for phases identification), used number of picks (No. of picks), Average rms traveltime misfit (rms) and normalized traveltime misfit (χ^2 error) for each phase.

Phase	No. of picks	rms	χ^2 error
Water	2441	0.039	0.155
Ps1	1731	0.061	0.369
PsP1	1383	0.066	0.441
PsP2	1015	0.076	0.578
Pg1	2898	0.099	0.744
Pg2	5918	0.071	0.458
PgP1	651	0.092	0.852
Pn	8085	0.066	0.429
Total	24 122	0.071	0.460

does not increase the rms error while it decreases significantly the number of explained traveltime picks. On the other hand, the rms error increases when thinning the crustal thickness without a drastic change in *F*-values. Therefore, the crustal thickness proposed in our model is the minimum acceptable thickness but it explains the largest number of traveltime picks, particularly the few observed PmP (Fig. 8).

7.4 Gravity modelling

A 2-D model consisting of homogeneous density blocks was constructed from the seismic velocity model. In the Algerian basin, a density of 2200, 2250 and 2330 kg m^{-3} is predicted from the velocity–density curve of Ludwig *et al.* (1970) for the sedimentary layers from top to bottom. A small increase to 2200, 2270 and 2350 kg m^{-3} is observed at the foot the margin. In the basin, the density of the upper and lower crust is 2700 and 2900 kg m^{-3}, respectively

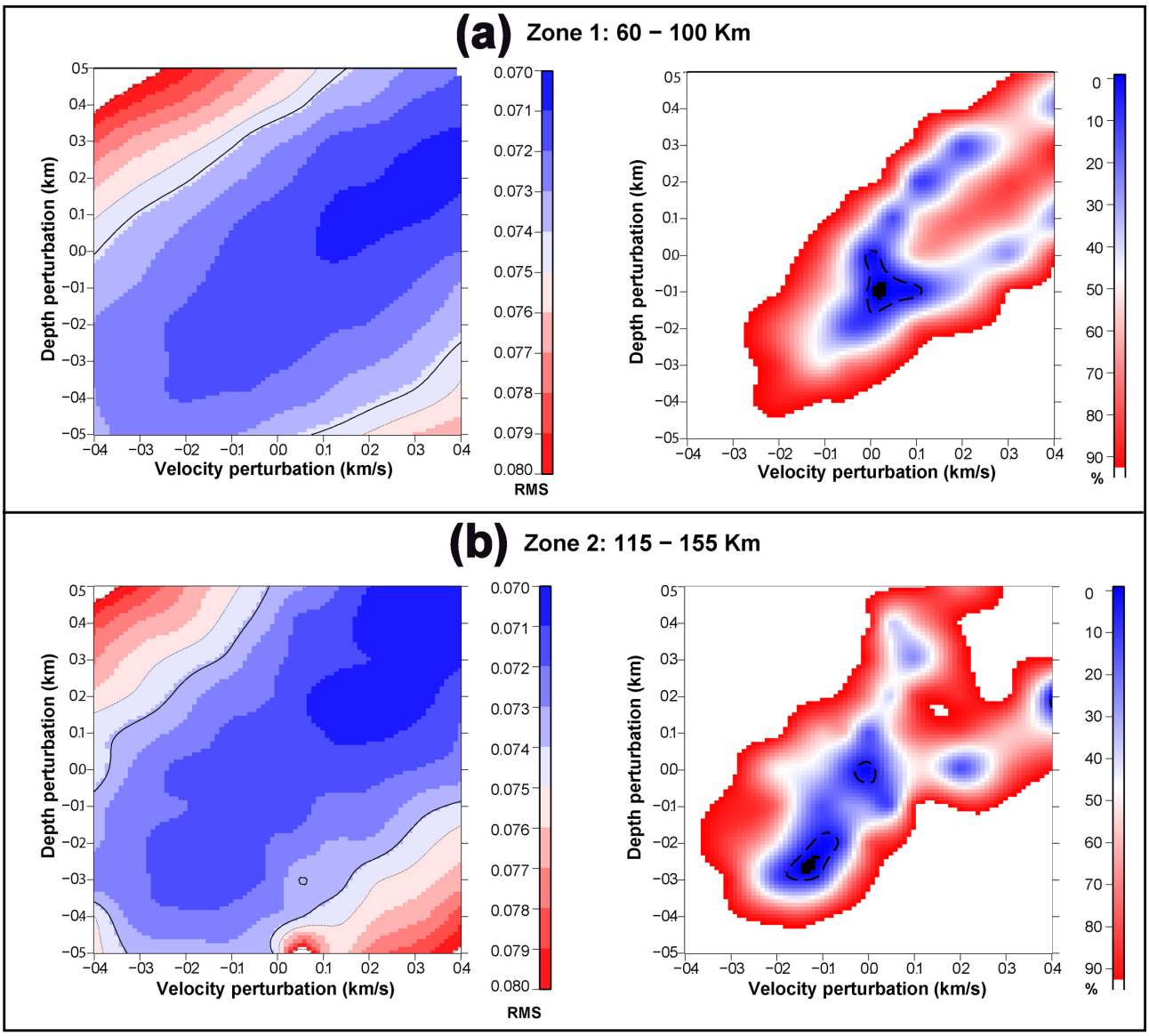

Figure 8. The rms error analysis and *F*-test by model perturbation in two 40-km-wide zones: (a) zone 1, between 60 and 100 km distance along profile (Fig. 7); (b) zone 2 between 115 and 155 km distance along profile (Fig. 7). The Moho depth is shifted between −0.5 and 0.5 km in each zone while kept at its original depth elsewhere in the model (with a 5 km wide taper); the lower crustal velocity at the Moho is shifted between −0.4 and 0.4 km s^{-1} in each zone. Left-hand panel: rms error of the calculated and observed traveltimes of OBS wide angle data. The 95 per cent confidence level is marked by a black contour. Right-hand panel: *F*-test percentage model significance deviation. The 5 per cent deviation is marked by a black contour.

Downloaded from https://academic.oup.com/gji/article/198/3/1486/583506 by CNRS - ISTO user on 19 October 2021

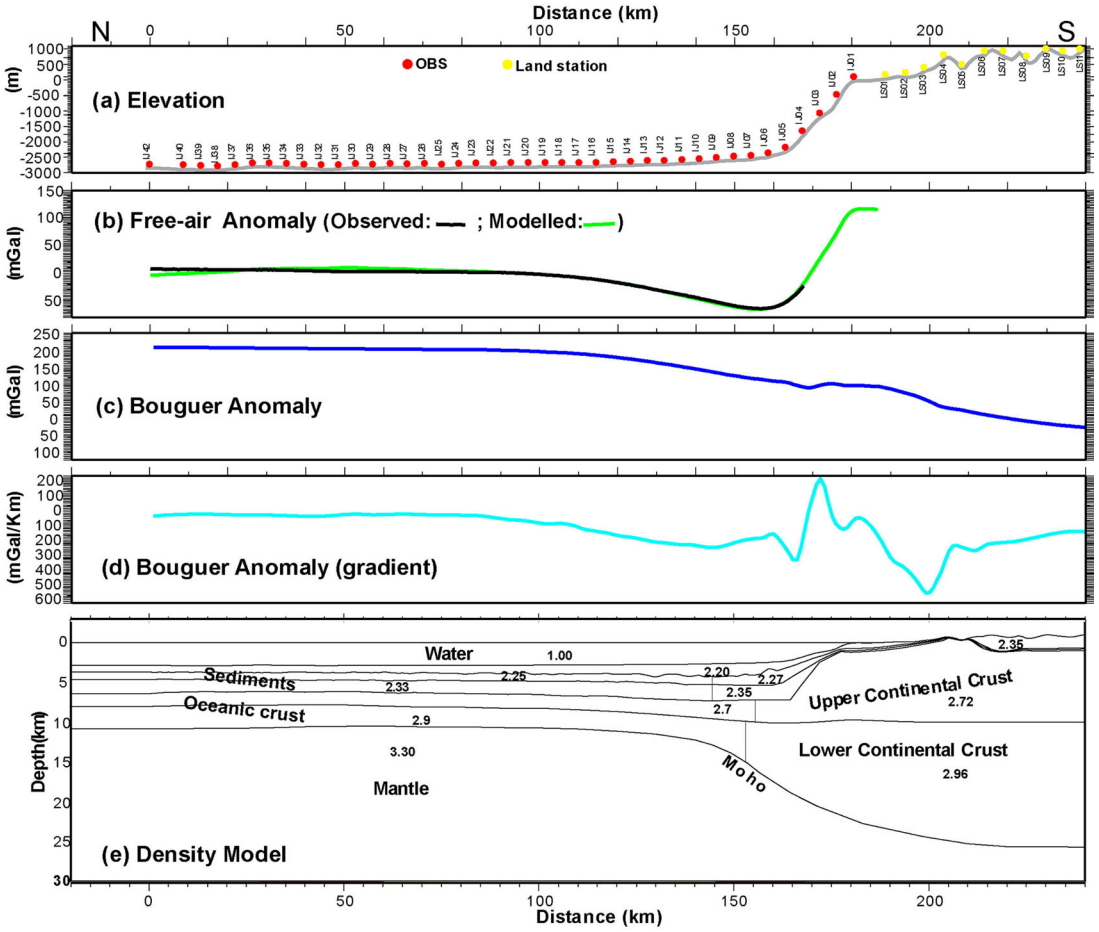

Figure 9. Results of gravity modelling. (a) Elevation data along the wide-angle profile. Positions of OBS are indicated by red circles and land stations by orange inverted triangles. (b) Observed free-air anomaly (black line) and the modelled anomaly (green line). (c) Observed Bouguer anomaly. (d) Horizontal gradient of Bouguer anomaly. (e) Densities converted from the velocity model (vertical exaggeration is 1.5). The model layer boundaries are defined directly from layer limits of the final velocity model (Fig. 6). Densities were computed using empirical velocity–density relationship of Ludwig *et al.* (1970). Continental crust densities were calculated using Christensen and Mooney's global compilation (1995). The mantle was defined as a single block of constant density of 3.3 kg m^{-3}. Densities used during the modelling are annotated.

(Fig. 9e). For the continental side, Christensen and Mooney velocity–density relationship (1995) predicts a density of 2720 and 2960 kg m^{-3} for the upper and lower crust layer in our model, respectively. Finally, the upper-mantle density is set at 3300 kg m^{-3}. The predicted free-air gravity anomaly from the density model shows a good fit with the shipboard measured anomaly (Fig. 9b) with a χ^2 error of 0.57, and a maximum deviation of 8.2 mGal at the northern extremity of the model. In the Algerian basin, between 0 and 130 km model distance, the density model is tabular (Fig. 9e), and the free-air anomaly is close to zero, indicating local isostatic equilibrium. To the south, the Moho depth increases from 11 to 25 km at the southern limit of the model, and accounts for the mass deficit responsible for the negative free-air anomaly and for the decrease in Bouguer gravity anomaly (Fig. 9c). The foot of the bathymetric slope coincides with the minimum of the free-air gravity anomaly and the bathymetric slope itself (Fig. 9a) coincides with a region characterised by positive gradients of the free-air anomaly (Fig. 9b). However, from the contact between the sedimentary basin at the foot of the margin and the Lesser Kabylia basement, between 165 and 170 km, the continental crustal mass-excess induces an increase in free-air anomaly, accompanied by a sharp decrease in the gradient of the Bouguer anomaly (Fig. 9c). Between 170 and 220 km, the Bouguer anomaly decreases to zero. Between 205 and 210 km, the Kabylian basement crops out and coincides with a local increase of the Bouguer anomaly gradient. South of 220 km, the Bouguer anomaly shows negative values, and presents a stable increase in the Bouguer anomaly gradient.

8 DISCUSSION

8.1 Seismic structure

In order to characterise the nature of the crust, 1-D velocity–depth profiles were extracted from the velocity model every 10 km. The individual and mean 1-D velocity profiles have been overlain on velocities bounds from typical oceanic and thinned continental crust. Based on comparisons of the layer thickness, relative layer thickness, seismic velocities and velocity gradients, the wide-angle transect shows four distinct domains from north to south (Fig. 10): (a) the deep sea oceanic basin from 0 to 130 km model distance, (b) the continent–ocean transition zone between 130 and 150 km, (c) the thinned continental crust and (d) the continental domain between 150 and 240 km. In these domains, specific tectono-sedimentary

Downloaded from https://academic.oup.com/gji/article/198/3/1486/583506 by CNRS - ISTO user on 19 October 2021

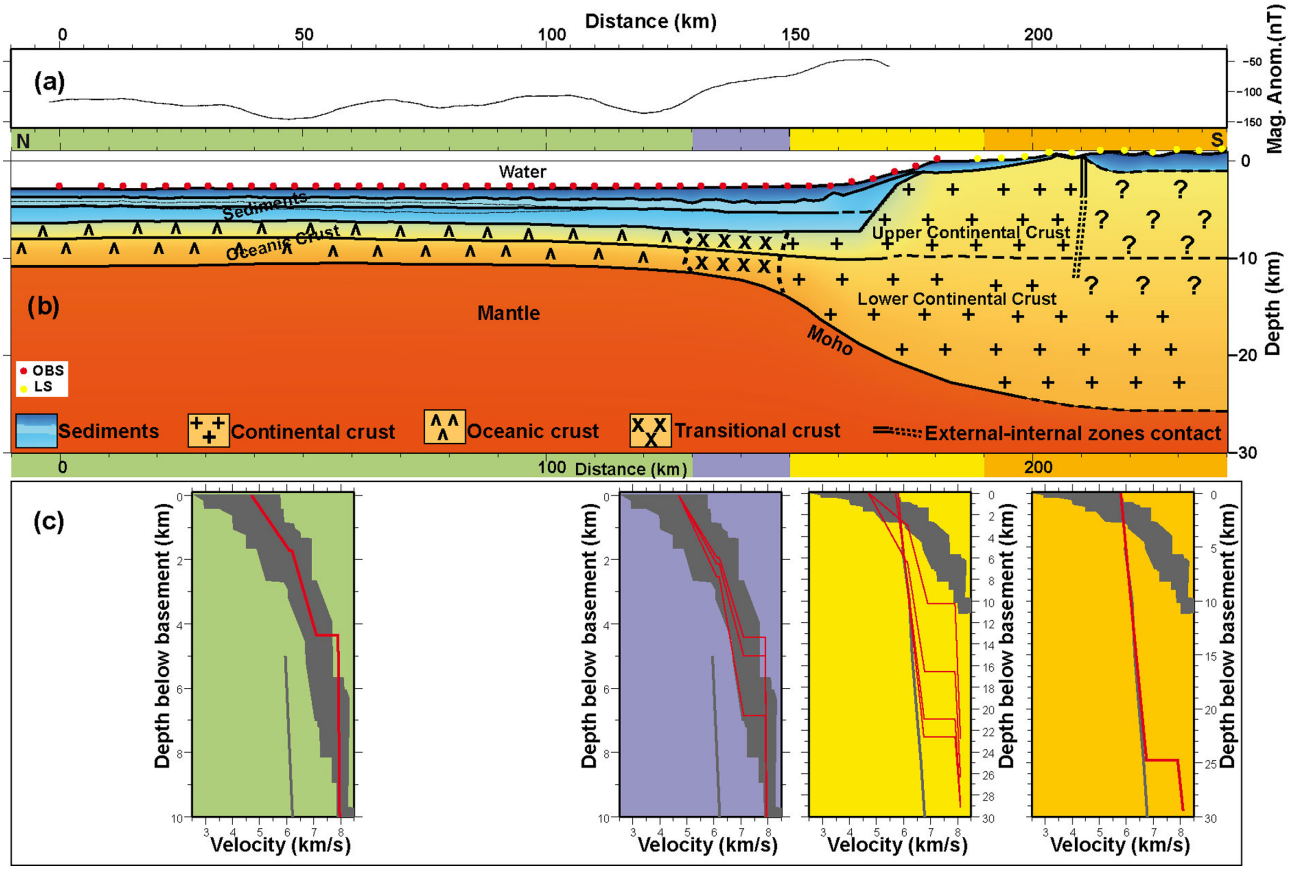

Figure 10. (a) Magnetic anomaly recorded along the profile, (b) final velocity model from forward modelling (vertical exaggeration is 2), (c) 1-D velocity–depth profiles and. Red circles indicate locations of the OBSs and land stations used in the modelling. 1-D velocity–depth profiles extracted every 10 km along the final velocity model and compared with pre-existing compilations of velocities–depth relations. White diagram (White *et al.* 1992) for oceanic crustal velocities, and Christensen and Mooney (1995) for continental crustal velocities. The oceanic zone is represented by green colour and the continental zone is in orange. The transitional oceanic–continental zone extends over blue and yellow domains.

features can be identified on the three industrial seismic profiles (Fig. 11).

Between 0 and 90 km distance along profile, the velocity model shows a tabular structuration. Below the seafloor, about 1 km thick undeformed Plio–Quaternary sediments have accumulated. Between 100 and 300-m-thick upper evaporites, appearing as a series of high amplitude sequence reflectors on the MCS profiles, seal the Messinian mobile unit. This approximately 1 km thick Messinian salt layer was modelled using a velocity up to 3.8 km s^{-1}, and presents very weak continuity on seismic images (Figs 4 and 11). In this area, the structure of the pre-Messinian sediments is poorly resolved but a velocity inversion is observed at the base of the MU with velocities ranging from 2.95 to 3.05 km s^{-1} at the top and 3.50 to 3.65 km s^{-1} at the bottom of the pre-Messinian units. The crust is separated into two distinct layers. The Moho is located at a depth of about 11 km and is characterised by a slight southward dip. Southward along the wide-angle profile, between 90 and 125 km, the dip of the Moho and crust further increases, together with that of the overlying pre-Messinian and Messinian units. The Plio-Quaternary sequence thickens to 1.5 km. This area is also characterised by the presence of well-expressed salt domes (Fig. 11). The seismic penetration improves and coherent reflections arise from sediments resting on the top of the crust. In this domain, few lateral variations are observed on the four MCS profiles (Figs 4 and 11).

The area between 125 and 157 km is characterised by the deepening of the top of the crust beneath sedimentary layers thickening from 4.5 to 5.5 km on profile L1–L3 (Fig. 11). The abyssal plain and the continental rise are made of a thick sedimentary sequence gathering several distinct sets: at the base, contact with the substratum is formed of a set of high seismic amplitude reflectors which are covered by a pre-Messinian sequence of relatively flat events. The MU forms a highly folded series showing strong salt tectonics, associated to Plio-Quaternary sediments waves. The internal structure of the MU is better imaged by the OBS records (Fig. 4d) than on the MCS profiles, probably because of its complex 3-D structure. The crustal thickness increases rapidly as the Moho depth increases to 16 km and acquires its maximum inclination at 158 km distance along the profile.

The transition from the deep basin to the continental shelf, between 157 and 172 km, is characterised by the thickening of Messinian units, the shallowest horizons appearing folded or tilted southward, but poorly resolved by the seismic imaging. Velocities in these sediments deposited at the foot of the margin are slightly lower than those located northward, indicating a lower salt content and a more detritic origin. While the seismic horizon representing the base of the MU disappears, the deeper pre-Messinian layers appear as flat horizons extending into contact with the continental crust. The upper continental crust thickens over a short distance: the top of the basement rises from 7 to 1.9 km depth, between OBS5

Downloaded from https://academic.oup.com/gji/article/198/3/1486/583506 by CNRS - ISTO user on 19 October 2021

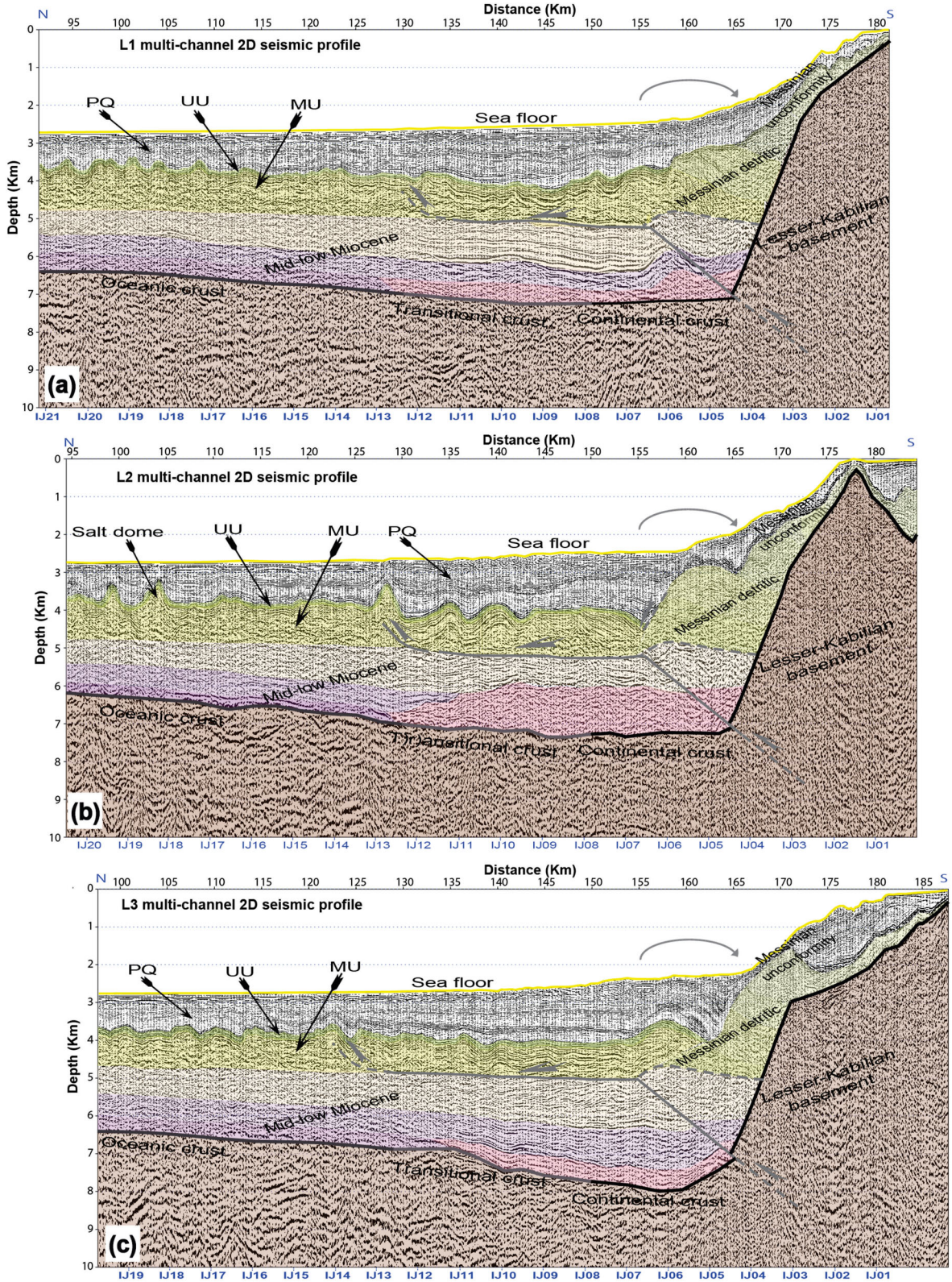

Figure 11. Depth converted pre-stack time migrated MCS profiles L1(a), L2(b) and L3(c), spaced every 15 km (see Fig. 1 for localization). Vertical exaggeration is 4. Time–depth conversion was performed using the velocity model from Spi14. The upper-evaporites units (UU), appears as a series of high amplitude sequences (with green colour) and seals the Messinian Mobile Unit (MU; with yellow colour). A lateral change in sedimentary thickness of 4.5–5.5 km (125–157 km MCS profiles distance) is observed from L1 to L3. The development of salt domes is apparent on the three profiles between 90 and 125 km. At the foot of the Lesser Kabylia basement between 155 and 165 km (and indicated by a bow arrow), a chaotic Messinian detritic unit appears to be landward dipping and overlain by Plio-Quaternary growth strata.

Downloaded from https://academic.oup.com/gji/article/198/3/1486/583506 by CNRS - ISTO user on 19 October 2021

and OBS4 spaced less than 4 km apart (Fig. 6). In this area, the Moho depth further increases from 19 to 21.5 km.

Between 175 and 205 km, the basin perched on the slope and continental shelf located between OBS02 and LS04, and partly imaged on profile L2 (Fig. 11b), likely consists mainly of Pliocene coastal marine sediments as proposed by Vila (1980). The thickness of the continental crust increases to 23 km. South of 195 km, the Moho is inferred to reach 25 km depth, based on its gently decreasing dip, but the maximum thickness of the continental crust is not resolved by this survey. Between land stations LS04 and LS06, the metamorphic Lesser Kabylia basement crops out, and is bordered by a series of Massylian flysch units. The wide-angle profile is located on the western boundary of the basement which extends eastward over 100 km (Bouillin 1977). At this location, the Lesser Kabylia basement limit is oblique to the margin and may therefore be almost vertical. Finally between 210 and 240 km, the model incorporates an approximately 3 km thick basin between land stations LS07 and LS11. At the surface, this zone was interpreted as Tellian nappes domain (Fig. 1). However, in the absence of seismic data characterizing the unit composing the suture, its precise structure remains undefined.

8.2 The Algerian basin

In the oceanic domain, two crustal layers have been modelled. The upper layer is characterised by a high velocity gradient between 4.7 and 6.1 km s^{-1} and a layer thickness of around 1.5 km and the lower layer by a lower velocity gradient between 6.2 and 7.1 km s^{-1} and a thickness of about 3 km. Although the complete crustal thickness is only between 4.5 and 5 km, clearly thinner than normal oceanic crust of 7 km (White *et al.* 1992), the relative layer thickness, the seismic velocities and velocity gradients are in good agreement with a crust accreted at an oceanic spreading centre, with layer 2 the basaltic layer and the underlying gabbroic layer 3. This low crustal thickness can be explained by two, non-exclusive, different scenarios, either accretion at very slow or ultra-slow spreading rates, where higher cooling rates lead to diminishing melt supply, or accretion in a back-arc basin setting. On one hand, numerical modelling shows that, at full spreading rates smaller than 20 mm a^{-1}, the crustal thickness decreases with spreading rate (Bown & White 1994). Very slow spreading rates might also explain the magnetic anomaly pattern of the Algerian basin. Most of the eastern Algerian basin is is characterised by irregular non-linear magnetic anomalies, which might origin from small volcanic centres rather than from a functioning spreading centre. Similar patterns can be found at slow and very slow spreading ridges, where the more magmatic segments produce magnetic anomalies, and amagmatic segments thinner crust producing subdued anomalies (Jokat & Schmidt-Aursch 2007). On the other hand crustal thickness in several backarc basins is reduced as compared to normal oceanic crust, such as the Liguro-Provençal basin or the Philippine Sea Basin (Louden 1980; Klingelhoefer *et al.* 2008; Gailler *et al.* 2009). Heat flow measurements in the Philippine Sea Basin indicate that the formation of thin crust is due to a thinner than normal lithosphere of 50–75 km (Louden 1980). In the case of the Algerian Basin, slow-spreading accretion in a backarc basin is also possible, as the Algerian basin is generally supposed to have formed in relation to the slab roll-back that eventually produced the separation between the Kabylies and the Alpine-Betics chain during Miocene times (Frizon de la Motte *et al.* 2000). The crustal structure (with thickness <5 km) and the absence of linear magnetic anomalies in the oceanic domain (Fig. 10) suggest analogies between the Algerian basin and the Liguro-Provençal basin. In both basins, the initiation of seafloor spreading is still a matter of debate. Based on geological evidence, seafloor spreading in the Algerian basin is considered to have occurred during the Aquitano-Burdigalian period (∼24–16 Ma) between the onset of plate separation between the Kabylides and the Balearic margin and the onset of collision between the Kabylies and the emplacement of the Flysh nappes. Global kinematic studies allow an estimate of the past Europe–Africa convergence rate (e.g. Fidalgo-Gonzales 2001; Schettino & Scotese 2005). Models reveal a N–S convergence between magnetic anomalies C24 et C13 (∼33 Ma, base of Oligocene), followed by a kinematic change to a NW–SE converge some-time between chron C13–C13n (∼33–33.1 Ma) and C6–C6n (∼20–19 Ma, Burdigalien). Schettino & Turco (2006) separate this change by two stage boundaries at 28.0 and 23.4 Ma: the first corresponds to the end of extension in the Valencia Trough and to the jump of the extensional centre towards the Balearic and Ligurian basins, and the second is associated with the start of rifting (and eventually seafloor spreading) in the eastern Algerian basin.

8.3 Transition zone and continental rift

The zone of transition between crust of oceanic nature and the continent is less than 20 km wide and might even be non-existent. No anomalous velocities higher than 7.1 km s^{-1} are imaged by the seismic data in this area as are frequently found on Atlantic Margins (Dean *et al.* 2000; Funck *et al.* 2004; Klingelhoefer *et al.* 2005) and which are proposed to consist of either serpentinized exhumed upper-mantle material, or underplated residues from volcanism. The continental crust is about 23 km thick, however we cannot exclude thickening of the crust towards the south, where it is not constrained by arrivals on the land station data. It is separated into two layers of similar thickness, which both are characterized by low velocity gradients and velocities typical for continental crust. At southern margin of the Balearic promontory, seismic Moho from three wide-angle profiles in the Algerian basin occurs at ∼11 km below sea level, reaching >24 km under SE Spain and Mallorca, and the COT is rather sharp without any evidence for exposed and serpentinized mantle in the transition zone (Grevemeyer *et al.* 2012). The crust in this region is of AlKaPeCa origin and therefore has an affinity to the European Plate. It might have been heavily reworked during its transition towards the African margin. In regard of the kinematic models, rifting of the Lesser Kabylia crust may have occurred in the context of an oblique Thetisian subduction, if it started after the kinematic change to a NW–SE convergence. At that time, an approximately 20° oblique subduction in the Lesser Kabylia forearc would exist, depending on the precise orientation of the trench, amount of trench retreat, and motion of the AlKaPeCa microblock. As a result, a trans-tensional regime might have prevailed during rifting, possibly leading to the formation of a transect of transform margin in the rear of the Lesser Kabylia. A transtensional rift would clearly best explain the sharp subvertical geometry of the Lesser Kabylia basement on the wide-angle profile (Fig. 10). Furthermore, oblique subduction often produces strain partitioning in the arc or forearc that can lead to lateral migration of large-scale forearc slivers, for instance at present-time in the Aleutian, Kuril, Nankai, southern Ryukyu, Philippine, southern Chile, Hikurangi, Lesser Antilles, New Britan or Sumatra Trenches (e.g. Fitch 1972; Beck 1983; Jarrard 1986; Kimura 1986; Curray 1989; DeMets 1992; McCaffrey 1992; Platt 1993; Lallemand *et al.* 1999). At the

Downloaded from https://academic.oup.com/gji/article/198/3/1486/583506 by CNRS - ISTO user on 19 October 2021

Kuril Trench (e.g. Kimura 1986) and Sumatra Trench (e.g. Curray 1989, 2005), a strike-slip system developed along the weakness of the arc lithosphere (e.g. the Central Sumatra fault). Therefore, strain partitioning might have preceded the extensional stage, and the continental rift might have inherited a pre-existing subvertical transform-fault system.

8.4 Steep and asymmetric continental margin

At the continental slope, the upper-crustal layer appears to thin more closely to the margin than the lower crustal layer. Hence, while the largest dip of the Moho is 23° at 155 km distance, the dip of the northern flank of the Kabylian basement reaches 32° at 168 km distance: about 13 km offsets maximal upper crustal from maximal lower crustal thinning. This asymmetric and depth dependent thinning can be observed on numerous other margins, for instance in the North Atlantic Ocean (e.g. Lavier & Manatschal 2006; Shillington *et al.* 2006; Péron-Pinvidic & Manatschal 2009; White & Smith 2009; Gerlings *et al.* 2012), the South China-Dangerous Grounds conjugate margins (Clift *et al.* 2002), or the central segment of the South Atlantic Ocean (e.g. Klingelhoefer *et al.* 2005; Aslanian *et al.* 2009; Blaich *et al.* 2011). Such an asymmetry in the geometry of the thinning of the upper and lower continental crust might be explained by either asymmetric rifting of the margin, an underplated body underneath the crust, or flow of lower crustal material towards the ocean basin.

1. The first hypothesis implies the decoupling between upper and lower crust at the initiation of the continental rifting, possibly inherited from the internal structure of the palaeo-Kabyle basement. An excess of upper continental crust, about 13 km × 4.75 km wide on our profile, would have drifted together with the conjugated margin or been abandoned at the foot of the Algerian margin during the early stages of rift in a mass-wasting process coined rotational slump as proposed for the Galicia Bank-Southern Iberian margin (Clark *et al.* 2007). On profile L2 (Fig. 11b) a 1-km-thick seismically disrupted body is imaged in the Algerian basin between 128 and 168 km on top of the thinned continental crust (not extending on the oceanic basin floor). The pre-Messinian sequence is conformable in this part of the basin and onlaps the allochthon disrupted body. Regionally, its thickness varies considerably along the margin foot. Such a body can be interpreted as syn-rift mass-wasting product of the former upper-continental crust. Alternatively, the body could have been emplaced later as an olistostrum during the accretion of Tethysian arc and the Lesser Kabylia to the Nubia margin around 19–16 Ma. The description of the origin and timing is difficult since small amounts and mainly pelagic sediments may have been deposited below this body. A similar allochthonous syn-rift body presenting a disrupted seismic facies has previously been observed at the foot of the North Biscay margin (Thinon *et al.* 2002).

2. Underplated bodies from volcanic activity are commonly found on highly volcanic margins, such as the Norwegian–Greenland margin, the Rockall Through (Mjelde *et al.* 1997; Klingelhoefer *et al.* 2005), or the Seychelles margin (Collier *et al.* 2009). However, these bodies are characterised by seismic velocities higher than continental crust and lower than upper-mantle material (7.4–7.8 km s^{-1}) and are identifiable by a double reflection from the top and base of the underplate body. Also, they are associated to large volcanic activity that is not observed along this part of the Algerian margin.

3. The third hypothesis implies a flow of lower crustal material towards the ocean basin. Numerical simulations of passive margin formation have predicted an oceanward flow of lower crustal material from under opposing conjugate margins (e.g. Sawyer & Harry 1991; Huismans & Beaumont 2002; Lavier & Manatschal 2006; Weinberg *et al.* 2007). In the case of transform margins, conduction of heat from the oceanic lithosphere to the adjacent continental lithosphere may produce uplift of the transform margin, and thinning of the continental crust by ductile flow of the lower crust towards the COT (Sage *et al.* 2000). Modelling of offset decoupling by Hopper and Buck (1998) shows that lower crustal flow might be expected for a range of heat flow values when the continental crust is 30 km thick, and when quartz is the dominant mineralogy, as is likely in the Lesser Kabylia basement.

8.5 Tectonic inversion of the Algerian margin

Kinematic studies indicate that present-day NW–SE convergence between the African and European plates is about 5.1 mm yr^{-1} at the longitude the wide-angle transect (Nocquet & Calais 2004; Stich *et al.* 2006). GPS data show that the Algerian Tell accommodates from 2.7 to 3.9 mm yr^{-1} of the present-day Nubia–Eurasia convergence, and that active shortening at rates ranging between 1.6 and 2.0 mm yr^{-1} is occurring between northern Africa and Iberia across the Algero-Balearic basin (Serpelloni *et al.* 2007) and even further north in the SE Iberian margin (Maillard & Mauffret 2011). The intense seismicity characterised by dominantly reverse-type fault plane moment tensors as well as folds and south-dipping blind thrusts observed offshore northern Algeria indicate that parts of the Algerian margin are undergoing a tectonic inversion (Déverchère *et al.* 2005; Yelles *et al.* 2009). On the MCS profiles between 157 and 167 km (Fig. 11), the Messinian detritic products that mass-wasted at the foot of the Lesser Kabylia basement, although very chaotic, appear to be landward dipping (Fig. 11). This unit forms a fold suggesting that the strata underwent tilt after its deposition against the basement. This unit is sealed by conformable seaward dipping slope deposit indicating that the tilting ceased shortly after deposition. The MU extend seaward forming a sharp contact with the detritic unit, ranging from an apparent normal fault and a progressive MU thinning on L1, to abrupt thinning of the MU mounted by rollover plio-Quaternary deposit on L2 (between 148 and 156 km) and L3 (between 153 and 164 km). These features clearly indicate a southward creep of the MU, which terminates into a well pronounced salt diapir located near 132 km on L1, 128 on L2 and 123 on L3. The pre-Messinian stata underneath appear mostly continuous, extending against the contact with the basement. Although the pre-Messinian units may not be preserved laterally and thickness increases eastward, these units also appear folded, with an axis located in the vicinity of 160 km on all profiles. This structure is the most compelling evidence for crustal shortening at the foot Algerian margin off Jijel and the presence of a thrust-fault emerging from the hinge of the Lesser Kabylia basin and basement rise. The MU diapirs and Plio-Quaternary roll-over structures seem to be mainly related to gravity driven northward creep of the mobile salt tong at the foot of the continental slope. However, the MU would also provide a relay from the thrust-fault in the pre-Messinian towards the diapir deforming the plio-Quaternary. Finally within the chaotic bodies that compose the glacis, seismic imaging suggests southward dipping units but data quality is not sufficient to reveal active thrusting of the basement rise. Southward, the sedimentary cover that rests on the steep slope of the margin is at most places too thin to evidence active shortening of the offshore Kabylian basement.

Downloaded from https://academic.oup.com/gji/article/198/3/1486/583506 by CNRS - ISTO user on 19 October 2021

9 CONCLUSIONS

The onshore-offshore combined modelling of wide-angle OBS and LS data and pre-stack depth migration of the seismic reflection data provides an unprecedented image of the deep structure along a 280 km long transect across the Algerian deep sea basin and continental margin. The Lesser Kabylian continental crust presents a sharp subvertical contact with the external zones. There, its thickness reaches 26 km. The crust thins to less than 5 km within less than 70 km: The continental shelf is narrow and has a very steep slope while the lower crust thins more seaward, suggesting an asymmetric and depth dependent thinning. Seaward in the deep sea basin, the crustal velocities evolve to two distinct layers of 4.7–6.1 and 6.2–7.1 km s^{-1}, typical of oceanic basins. The ocean–continent transition zone is very narrow, between 15 and 20 km. The Algerian basin basement presents a southward slope, with total sediment thickness decreasing from about 4.5 to 5.5 km at the foot of the Kabylian basement to 3.75 km towards the northern end of our profile. In our study area, large lateral changes are found among the units deposited at the foot of the Kabylian basement, suggesting that mass-wasting processes were dominant in the period between rifting and the accretion of the Lesser Kabylia to Africa. Later during the Messinian salinity crisis, up to 3 km of detritic deposits accumulated against the basement slope. Since then, the structures of the foot of the Algerian basin appear dominated by gravity driven salt tectonics, showing northward creep of the MU and the formation of salt diapirs towards the northern part of the MCS profiles. Deformation within the pre-Messinian units, as imaged on the seismic data presented in this study, indicates active thrusting of the crust at the base of the continental slope and tectonic inversion of the Algerian margin off the lesser Kabylia.

ACKNOWLEDGEMENTS

We are truly grateful to the captain and crew of the N/V l'Atalante. We wish to thank also the OBS team of Ifremer-UBO and the Genavir seismic team for their dedication at sea. We wish to acknowledge SONATRACH (National oil company, Algeria) and ALNAFT (Agence Nationale pour la Valorisation des Ressources en Hydrocarbures, Algeria) to allow us to use and publish the additional seismic lines. The MCS profiles were processed using the Geocluster (CGG Veritas), and Seismic Unix (Stockwell 1999a,b) processing software. The GMT (Generic Mapping Tool) software was used in the preparation of most figures (Wessel & Smith 1995). The Rayinvr software (Zelt & Smith 1992) was used for ray tracing modelling of the wide-angle seismic data.

REFERENCES

Aidi, C. *et al.*, 2013. Deep structure of the Algerian margin offshore Great Kabylie: preliminary results of an offshore-onshore seismic profile (SPIRAL campaign), in Paper *EGU2013–7729 presented at EGU General Assembly*, Vienna, Austria, 7–12 April.

Aslanian, D. *et al.*, 2009. Brasilian and Angolan passive margins: the kinematic constraints, *Tectonophysics,* **468,** 98–112.

Avedik, F., Renard, V., Allenou, J. & Morvan, B., 1993. "Single bubble" airgun array for deep exploration, *Geophysics,* **58,** 366–382.

Badji, R. *et al.*, 2013. Geophysical evidence for a transform margin in Northwestern Algeria: possible vestige of a Subduction-Transform Edge Propagator, *AGU Fall Meeting Abstracts,* **-1,** 2515.

Beck, M.E., 1983. On the mechanism of tectonic transport in zones of oblique subduction, *Tectonophysics,* **93,** 1–11.

Benali, H., 2007. Les minéralisations associées aux roches magmatiques tertiaires du Nord de l'Algérie: typologie, pétrologie, cadre géodynamique et implication métallogénique, *PhD thesis,* USTHB, Algerie.

Benson, R.H., Rakic-El Bied, K. & Bonaduce, G., 1991. An important current reversal (influx) in the Rifian Corridor (Morocco) at the Tortonian-Messinian boundary: the end of the Tethys Ocean, *Paleoceanography,* **6**(1), 164–192.

Blaich, O.A., Faleide, J.I. & Tsikalas, F., 2011. Crustal breakup and continent ocean transition at South Atlantic conjugate margins, *J. geophys. Res.,* **116,** B01402, doi:10.1029/2010JB007686.

Bouillin, J.P., 1977. Gelogie alpine de la Lesser Kabylia dans dans les régions de Collo et d'El Milia, *PhD thesis,* Univ. Piere et Marie Curie, France.

Bouillin, J.P., 1986. Le bassin maghrébin: une ancienne limite entre l'Europe et l'Afrique à l'ouest des Alpes, *Bulletin De La Societe Geologique De France,* **8**(4), 547–558.

Bouillin, J.P. & Raoult, J.F., 1971. Présence sur le socle kabyle du Constantinois d'un olistrostrome lié au charriage des flyschs. Le Numidien peut-il être un néo-autochtone? *Bull. Soc. Géol., France,* **XIII**(7), 338–336.

Bouillin, J.P., Kornprobst, J. & Raoult, J.F., 1977. Données préliminaires sur le complexe volcano-sedimentaire de Rekkada Metlefine (Ex-Texenna) en Petite Kabylie (Algerie), *Bull. Sot. Geol. Fr.,* **19,** 805–813.

Bouyahiaoui, B. *et al.*,2013. Deep structure of the Easternmost part of the Algerian margin and adjacent deep basin in Annaba Region deduced from wide-angle modelling and multichannel seismic data, *AGU Fall Meeting Abstracts,* **-1,** 2539.

Bown, J. & White, R.S., 1994. Variation with spreading rate of oceanic crustal thickness and geochemistry, *Earth planet. Sci. Lett.,* **121**(3–4), 999–1015.

Calais, E., DeMets, C. & Nocquet, J.M., 2003. Evidence for a post-3.16-Ma change in Nubia-Eurasia-North America plate motions? *Earth planet. Sci. Lett.,* **216,** 81–91.

Christensen, N.I. & Mooney, W.D., 1995. Seismic velocity structure and composition of the continental-crust—a global view, *J. geophys. Res.-Solid Earth,* **100**(B6), 9761–9788.

Clark, S.A., Sawyer, D.S., Austin, J.A. Jr., Christeson, G.L. & Nakamura, Y., 2007. Characterizing the Galicia Bank-Southern Iberia Abyssal Plain rifted margin segment boundary using multichannel seismic and ocean bottom seismometer data, *J. geophys. Res.,* **112,** B03408, doi:10.1029/2006JB004581.

Clift, P., Lin, J. & Barckhausen, U., 2002. Evidence of low flexural rigidity and low viscosity lower continental crust during continental break-up in the South China Sea, *Mar. Petrol. Geol.,* **19,** 951–970.

Collier, J.S., Minshull, T.A., Hammond, J.O.S., Whitmarsh, R.B., Kendall, J.M., Sansom, V., Lane, C.I. & Rumpker, G., 2009. Factors influencing magmatism during continental breakup: new insights from a wide-angle seismic experiment across the conjugate Seychelles-Indian margins, *J. geophys. Res.,* **114,** b03101, doi:10.1029/2008jb005898.

Curray, J.R., 1989. The Sunda Arc: a model for oblique plate convergence, *Neth. J. Sea Res.,* **24,** 131–140.

Curray, J.R., 2005. Tectonics and history of the Andaman Sea region, *J. Asian Earth Sci.,* **25,** 187–232.

Dash, R., Spence, G., Hyndman, R., Grion, S., Wang, Y. & Ronen, Shuki., 2009. Wide-area imaging from OBS multiples, *Geophysics,* **74**(6), Q41–Q47.

Dean, S.M., Minshull, T.A., Whitmarsh, R.B. & Louden, K.E., 2000. Deep structure of the ocean-continent transition in the southern Iberia Abyssal Plain from seismic refraction profiles: the IAM-9 transect at 40°20′N, *J. geophys. Res.-Solid Earth,* **105**(B3), 5859–5885.

DeMets, C., 1992. Oblique convergence and deformation along the Kuril and Japan trenches, *J. geophys. Res.,* **97,** 17 615–17 626.

Déverchère, J. *et al.*, 2005. Active thrust faulting offshore Boumerdes, Algeria, and its relations to the 2003 Mw 6.9 earthquake, *Geophys. Res. Lett.,* **32,** L04311, doi:10.1029/2004GL021646.

Djelit, H., 1987. Evolution tectono-metamorphique du socle Kabyle et polarité de mise en place des nappes de flysch enpetite Kabylie occidentale (Algerie), *PhD thesis,* Univ. Paris-sud, Centre D'Orsay, France.

Downloaded from https://academic.oup.com/gji/article/198/3/1486/583506 by CNRS - ISTO user on 19 October 2021

Domzig, A. *et al.*, 2006. Searching for the Africa-Eurasia miocene boundary offshore Western Algeria (maradja'03 cruise), *Comptes Rendus Geoscience,* **338**(1–2), 80–91.

Durand-Delga, M. & Fontboté, J.M., 1980. Le cadre structural de la Méditerranée occidentale, *Intern. Geol. Congr. 26th,* **C5,** 67–85.

Fidalgo-Gonzales, L., 2001. La cinématique de L'Atlantique Nord : la question de la déformation intraplaque, *PhD thesis,* Université de Bretagne Occidentale, pp 1–340.

Fitch, T.J., 1972. Plate convergence, transcurrent faults and internal deformation adjacent to southeast Asia and the western Pacific, *J. geophys. Res.,* **84,** 4432–4460.

Fowler, C.M.R., 1990. *The Solid Earth: An Introduction to Global Geophysics,* Cambridge Univ. Press.

Frizon de Lamotte, D., Saint Bezar, B.A., Bracene, R. & Mercier, E., 2000. The two main steps of the atlas building and geodynamics of the Western Mediterranean, *Tectonics,* **19**(4), 740–761.

Funck, T., Jackson, H.R., Louden, K.E., Dehler, S.A. & Wu, Y., 2004. Crustal structure of the northern Nova Scotia rifted continental margin (eastern Canada), *J. geophys. Res.-Solid Earth,* **109**(B9), doi:10.1029/2004JB003008.

Gailler, A., Klingelhoefer, F., Olivet, J.L. & Aslanian, D., 2009. Crustal structure of a young margin pair: new results across the Liguro–Provencal Basin from wide-angle seismic tomography, *Earth planet. Sci. Lett.,* **286,** 333–345.

Gautier, F., Clauzon, G., Suc, J.P., Cravatte, J. & Violanti, D., 1994. Age and duration of the Messinian salinity crisis, *Comptes Rendus De L Academie Des Sciences Serie Ii,* **318**(8), 1103–1109.

Gerlings, J., Louden, K.E., Minshull, T.A. & Nedimovic, M.R., 2012. Flemish Cap-Goban Spur conjugate margins: new evidence of asymmetry, *Geology,* **40,** 1107–1110.

Govers, R., 2009. Choking the Mediterranean to dehydration: the Messinian salinity crisis, *Geology,* **37,** 167–170.

Grevemeyer, I., Ranero, C.R., Pesquer, D. & Gallart, J., 2012. Slab rollback and continental break-up in a convergent setting seismic structure of passive continental margins in the Western Mediterranean Sea, in *Proceedings of the EGU General Assembly*, Vienna, Austria, 22–27 April, p. 8795.

Harbi, A., Maouche, S. & Ayadi, A., 1999. Neotectonics and associate seismicity in the Eastern Tellian, *J. Seismol.,* **3,** 95–104.

Harbi, A., Benouar, D. & Benhallou, H., 2003. Re-appraisal of seismicity and seismotectonics in the north-eastern Algeria Part I: review of historical seismicity, *J. Seismol.,* **7,** 115–136.

Hopper, J.R. & Buck, W.R., 1998. Styles of extensional decoupling, *Geology,* **26,** 699–702.

Hsü, K.J., Cita, M.B. & Ryan, W.B.F., 1973. The origin of the Mediterranean evaporites, *Init. Rept. Deep Sea Drill. Proj.,* **13,** 1203–1231.

Huismans, R.S. & Beaumont, C., 2002. Asymmetric lithospheric extension: the role of frictional-plastic strain softening inferred from numerical experiments, *Geology,* **30,** 211–214.

Jarrard, R.D., 1986. Terrane motion by strike-slip faulting of fore-arc slivers, *Geology,* **14,** 780–783.

Jokat, W. & Schmidt-Aursch, M.C., 2007. Geophysical characteristics of the ultraslow spreading Gakkel Ridge, Arctic Ocean, *Geophys. J. Int.,* **168**(3), 983–998.

Kherroubi, A. *et al.*, 2009. Recent and active deformation pattern off the easternmost Algerian margin, Western Mediterranean Sea: new evidence for contractional tectonic reactivation, *Mar. Geol.,* **261,** 17–32.

Kimura, G., 1986. Oblique subduction and collision: forearc tectonics of the Kuril arc, *Geology,* **14**(5), 404–407.

Klingelhoefer, F. *et al.*, 2008. Preliminary results from the Sardinia deep seismic cruise on the Western Sardinia and Gulf of Lions conjugate margin pair, in *Proceedings of the EGU General Assembly Meeting,* Vienna, April.

Klingelhoefer, F., Edwards, R.A., Hobbs, R.W. & England, R.W., 2005. Crustal structure of the ne rockall trough from wide-angle seismic data modelling, *J. geophys. Res.-Solid Earth,* **110**(B11), doi:10.1029/2005JB003763.

Krijgsman, W., Hilgen, F.J., Raffi, I., Sierro, F.J. & Wilson, D.S., 1999. Chronology, causes and progression of the Messinian Salinity Crisis, *Nature,* **400**(6745), 652–655.

Lallemand, S.E., Liu, C.S., Dominguez, S., Schnurle, P. & Malavieille, J., 1999. Trench-parallel stretching and folding of forearc basins and lateral migration of the accretionary wedge in the southern Ryukyus: a case of strain partition caused by oblique convergence, *Tectonics,* **18,** 231–247.

Lavier, L. & Manatschal, G., 2006. A mechanism to thin the continental lithosphere at magma-poor margins, *Nature,* **440,** 324–328.

Leprêtre, A., Klingelhoefer, F., Graindorge, D., Schnurle, P., Beslier, M.O., Yelles, K., Déverchère, J. & Bracene, R., 2013. Multiphased tectonic evolution of the Central Algerian margin from combined wide-angle and reflection seismic data off Tipaza, Algeria, *J. geophys. Res.-Solid Earth,* **118,** 1–18.

Liu, Z. & Bleisten, N., 1995. Migration velocity analysis: theory and an iterative algorithm, *Geophysics,* **60,** 142–153.

Lofi, J. *et al.*, 2011. Refining our knowledge of the Messinian salinity crisis records in the offshore domain through multi-site seismic analysis, *Bull. Soc. géol. France,* **182**(2), 163–180.

Louden, K.E., 1980. The crustal and lithospheric thicknesses of the Philippine Sea as compared to the Pacific, *Earth planet. Sci. Lett.,* **50**(1), 275–288.

Ludwig, W.J., Nafe, J.E. & Drake, C.L., 1970. Seismic refraction, in *The Sea,* Vol. 4, pp. 53–84, ed. Maxwell, A.E., Wiley.

Lutter, W.J. & Nowack, R.L., 1990. Inversion for crustal structure using reflections from the PASSCAL Ouachita experiment, *J. geophys. Res.,* **95,** 4633–4646.

Mahdjoub, Y., 1990. Cinématique des déformations tertiaires dans le massif de la Petite Kabylie (Algérie orientale), *Bull. Sol. géol. France.,* **8**(VI), 629–634.

Maillard, A. & Mauffret, A., 2011. Structure and present-day compression in the offshore area between Alicante and Ibiza Island (Eastern Iberian Margin), *Tectonophysics,* **591,** 116–130.

Mauffret, A., Frizon de Lamotte, D., Lallemant, S., Gorini, C. & Maillard, A., 2004. E-W opening of the Algerian Basin (Western Mediterranean), *TerraNova,* **16,** 257–264.

Mauffret, A., Ammar, A., Gorini, C. & Jabour, H., 2007. The Alboran Sea (Western Mediterranean) revisited with a view from the Moroccan margin, *Terra Nova,* **19**(3), 195–203.

Maury, R.C. *et al.*, 2000. Post-collisional Neogene magmatism of the Mediterranean Maghreb margin; a consequence of slab breakoff, *Comptes Rendus de l'Académie des Sciences,* **331,** 159–173.

McCaffrey, R., 1992. Oblique plate convergence, slip vectors, and fore-arc deformation, *J. geophys. Res.,* **97,** 8905–8915.

Mjelde, R., Kodaira, S., Shimamura, H., Kanazawa, T., Shiobara, H., Berg, E.W. & Riise, O., 1997. Crustal structure of the central part of the Vøring Basin, mid-Norway margin from ocean bottom seismographs, *Tectonophysics,* **277,** 235–257.

Nocquet, J.M. & Calais, E., 2004. Geodetic measurements of crustal deformation in the Western Mediterranean and Europe, *Pure appl. Geophys.,* **161**(3), 661–681.

Péron-Pinvidic, G. & Manatschal, G., 2009. The final rifting evolution at deep magma-poor passive margins from Iberia–Newfoundland: a new point of view, *Int. J. Earth Sci.,* **98,** 1581–1597.

Platt, J.P., 1993. Mechanics of Oblique Convergence, *J. geophys. Res.,* **98,** 16 239–16 256.

Raoult, J.F., 1969. Nouvelles données sur les flyschs au Nord du Rif Sidi Driss et dans la zone du Col des Oliviers (Nord du Constantinois, Algérie), *Bull. Soc. Géol. France,* **7**(XI), 516–543, 2 fig.

Raoult, J., 1975. Évolution paléogéographique et structurale de la Chaine alpine entre le Golf de Skikda et Constantine (Algérie Orientale), *Bull. Soc. Geol. France,* **XVII**(7), 394–409, 6 fig.

Rosenbaum, G. & Lister, G.S., 2004. Neogene and Quaternary rollback evolution of the Tyrrhenian Sea, the Apennines and the Sicilian Maghrebides, *Tectonics,* **23,** TC1013, doi:10.1029/2003TC001518.

Rosenbaum, G., Lister, G.S. & Duboz, C., 2002. Reconstruction of the evolution of the Alpine-Himalayan Orogen, *J. Virtual Explor.,* **8,** 107–130.

Downloaded from https://academic.oup.com/gji/article/198/3/1486/583506 by CNRS - ISTO user on 19 October 2021

Sage, F., Basile, Ch., Mascle, J., Pontoise, B. & Whitmarsh, R.B., 2000. Crustal structure of the continent-ocean transition off the côte d'Ivoire-Ghqnq tranform margin: implications for thermal exchanges across the palaeotransform boundary, *Geophys. J. Int.,* **143,** 662–678.

Sawyer, D.S. & Harry, D.L., 1991. Dynamic modelling of divergent margin formation; application to the US Atlantic margin, *Mar. Geol.,* **102,** 29–42.

Serpelloni, E., Vannucci, G., Pondrelli, S., Argnani, A., Casula, G., Anzidei, M., Baldi, P. & Gasperini, P., 2007. Kinematics of the Western Africa-Eurasia plate boundary from focal mechanisms and GPS data, *Geophys. J. Int.,* **169**(3), 1180–1200.

Schettino, A. & Scotese, C.R., 2005. Apparent polar wander paths for the major continents (200 Ma - Present Day): a paleomagnetic reference frame for global plate tectonic reconstructions, *Geophys. J. Int.,* **163**(2), 727–759.

Schettino, A. & Turco, E., 2006. Plate kinematics of the Western Mediterranean region during the Oligocene and Early Miocene, *Geophys. J. Int.,* **166,** 1398–1423.

Schneider, W.A. & Backus, M., 1964. Ocean-bottom seismic measurements off the California coast, *J. geophys. Res.* **69**(6) 1135–1143.

Shillington, D.J., Holbrook, W.S., Van Avendonk, H.J.A., Tucholke, B.E., Hopper, J.R., Louden, K.E., Larsen, H.C. & Nunes, G.T., 2006. Evidence for asymmetric nonvolcanic rifting and slow incipient oceanic accretion from seismic reflection data on the Newfoundland margin, *J. geophys. Res.,* **111,** B09402, doi:10.1029/2005JB003981.

Speranza, F., Villa, I.M., Sagnotti, L., Florindo, F., Cosentino, D., Cipollari, P. & Mattei, M., 2002. Age of the Corsica-Sardinia rotation and Liguro-Provencal basin spreading: new paleornagnetic and Ar/Ar evidence, *Tectonophysics,* **347**(4), 231–251.

Stich, D., Serpelloni, E., Mancilla, F.D. & Morales, J., 2006. Kinematics of the Iberia-Maghreb plate contact from seismic moment tensors and gps observations, *Tectonophysics,* **426**(3–4), 295–317.

Stockwell, J.W. Jr. 1999a. The cwp/su: seismic Unix package, *Comput. Geosci.,* **25**(4), 133–419.

Stockwell, J.W. Jr., 1999b. Free software in education: a case study of CWP/SU: Seismic Unix, *Leading Edge,* **61**(3), 759–775.

Thinon, I., Réhault, J.P. & Fidalgo-Gonzales, L., 2002. La couverture sédimentaire syn-rift de la marge Nord-Gascogne et du Bassin armoricain (golfe de Gascogne): à partir de nouvelles données de sismique réflexion, *Bull. Soc. géol. Fr.,* **173**(6), 515–522.

Vila, J.P., 1980. La chaine alpine d'Algerie orientale et des confins Algero-Tunisien, *PhD thesis,* Univ. Piere et Marie Curie (Paris VI), France.

Weinberg, R.F., Regenauer-Lieb, K. & Rosenbaum, G., 2007. Mantle detachments and the break-up of cold continental crust, *Geology,* **35,** 1035–1038.

Wessel, P. & Smith, W.H.F., 1995. New version of the generic mapping tools released, *EOS, Trans. Am. geophys. Un.,* **76**(33), 329, doi:10.1029/95EO00198.

White, R.S. & Smith, L.K., 2009. Crustal structure of the Hatton and the conjugate east Greenland rifted volcanic continental margins, NE Atlantic, *J. geophys. Res.,* **114,** B02305, doi:10.1029/2008JB005856.

White, R.S., McKenzie, D. & Onions, R.K., 1992. Oceanic crustal thickness from seismic measurements and rare-earth element inversions, *J. geophys. Res.-Solid Earth,* **97**(B13), 19 683–19 715.

Wildi, W., 1983. La chaîne tello rifaine (Algérie, Maroc, Tunisie): structure, stratigraphie et évolution du Trias au Miocène, *Rev. Géol. Dyn. géog. Phys.,* **24**(3), 201–297.

Yelles, C.A., Roger, J., Déverchère, J., Bracène, R., Domzig, A., Hèbert, H. & Kherroubi, K., 2009. The 1856 tsunami of Djidjelli (Eastern Algeria): seismotectonics, modelling and hazard implications for the Algerian coast, *Pure appl. geophys.,* **166,** 283–300.

Zelt, C.A., 1999. Modelling strategies and model assessment for wide-angle seismic traveltime data, *Geophys. J. Int.,* **139,** 183–204.

Zelt, C.A. & Smith, R.B., 1992. Seismic traveltime inversion for 2-D crustal velocity structure, *Geophys. J. Int.,* **108,** 16–34.

Downloaded from https://academic.oup.com/gji/article/198/3/1486/583506 by CNRS - ISTO user on 19 October 2021